DOKUZ EYLÜL UNIVERSITY
GRADUATE SCHOOL OF NATURAL AND APPLIED SCIENCES

INVESTIGATION OF SOLIDIFICATION AND MELTING PERIODS OF PHASE CHANGE MATERIALS INSIDE CAPSULES

by

Servet Giray HACIPAŞAOĞLU

June, 2019

İZMİR

INVESTIGATION OF SOLIDIFICATION AND MELTING PERIODS OF PHASE CHANGE MATERIALS INSIDE CAPSULES

A Thesis submitted to the
Graduate School of Natural Sciences of Dokuz Eylül University
In Partial Fulfillment of the Requirements for the Degree of Master of Science in Mechanical Engineering, Thermodynamics Program

by

Servet Giray HACIPAŞAOĞLU

June, 2019

İZMİR

M.Sc THESIS EXAMINATION RESULT FORM

We have read the thesis entitled **"INVESTIGATION OF SOLIDIFICATION AND MELTING PERIODS OF PHASE CHANGE MATERIALS INSIDE CAPSULES"** completed by **SERVET GİRAY HACIPAŞAOĞLU** under supervision of **ASSOC. PROF. DR. MEHMET AKİF EZAN** and we certify that in our opinion it is fully adequate, in scope and in quality, as a thesis for the degree of Master of Science.

Assoc. Prof. Dr. Mehmet Akif EZAN

Supervisor

Prof.Dr. Aytunç EREK

Jury Member

Asst. Prof. Dr. Levent BİLİR

Jury Member

Prof. Dr. Kadriye ERTEKİN

Director

Graduate School of Natural and Applied Sciences

ACKNOWLEDGEMENTS

I would like to thank my advisor, Assoc. Prof. Dr. Mehmet Akif EZAN, for his effort of this work and his willing to teach which I always admire.

I also thank the technician Alim ZORLUOL providing his expertise to experiments and this thesis.

The experimental setup used in this thesis was established within the scope of TÜBITAK 112M164 project. I would like to thank TÜBİTAK and Prof. Dr. Aytunç EREK for their support.

I would also like to express my special thanks to Merve KAYA, for her endless helps for this study and me.

Finally, I would like to thank my family for their encouragements. They always support my decisions. I wish to express my gratitude to them because of their patience.

Servet Giray HACIPAŞAOĞLU

INVESTIGATION OF SOLIDIFICATION AND MELTING PERIODS OF PHASE CHANGE MATERIALS INSIDE CAPSULES

ABSTRACT

The current thesis consists of two parts as experimental and numerical. In the experimental part, the storage performance of spherical encapsulated phase change material (PCM) under various external boundary conditions was obtained experimentally. As the charging performance of spherical encapsulated PCM is achieved, the entry velocity of the heat transfer fluid (HTF) into the test zone is kept constant and the entry temperature is changed. The effect of changing HTF temperatures on the change in temperature of the capsule and the heat transfer rate were investigated.

In the numerical part, the influences of inlet temperature and velocity of the HTF and the capsule material on the performance of a latent heat thermal energy storage unit is numerically investigated. The enhanced thermal conductivity approach is implemented into the ANSYS-FLUENT software to consider the natural-convection-dominated melting process within the capsules. Results of the parametric analyses are evaluated by using the first and second laws of the thermodynamics. The time-wise variations of the melting front, the temperature of the PCM and the rate of entropy generation are evaluated. Increasing the inlet temperature and velocity of air significantly reduces the time required for complete melting. The total time for melting is reduced when the inlet temperature of air increase and the entropy generation rate enhances more than four times. Besides, increasing the air inlet velocity enhances the entropy generation.

Keywords: Inward melting, spherical capsules, enhanced thermal conductivity, phase change materials

KAPSÜLLER İÇERİSİNDEKİ FAZ DEĞİŞİM MALZEMELERİNİN KATILAŞMA VE ERİME PERİYOTLARININ İNCELENMESİ

ÖZ

Bu tez çalışması, deneysel ve sayısal olarak iki bölümden oluşmaktadır. Deneysel çalışmada küresel kapsüllenmiş faz değişim malzemesinin (FDM) çeşitli dış ortam sınır koşullarında depolama performansı deneysel olarak elde edilmiştir. Küresel kapsüllenmiş FDM'nin depolama performansı elde edilirken, ısı transfer akışkanının (ITA) test alanına giriş hızı sabit tutulmuş ve giriş sıcaklığı değiştirilmiştir. Değişen ITA sıcaklıklarının kapsül sıcaklığında ve ısı transfer hızında oluşturduğu değişimler incelenmiştir.

Sayısal çalışmada, ITA'nın hızı, giriş sıcaklığı ve kapsül malzemesinin değişiminin gizli bir ısıl enerji depolama ünitesinin performansı üzerindeki etkileri sayısal olarak incelenmiştir. Etkin ısıl iletkenlik yaklaşımı, kapsüller içindeki doğal taşınımlı erime işlemini dikkate almak için ANSYS-FLUENT yazılımına uygulanmıştır. Parametrik analizlerin sonuçları, termodinamiğin birinci ve ikinci yasaları dikkate alınarak oluşturulmuştur. Erime prosesinin zamana bağlı değişimleri, FDM'nin sıcaklığı ve entropi üretim oranı değişimleri değerlendirilmiştir. Giriş sıcaklığının ve havanın hızının arttırılması, tam erime süresini önemli ölçüde azalttığı gözlenmiştir. Havanın giriş sıcaklığı yükseldiğinde ve entropi üretim oranı dört kattan fazla arttığında, toplam erime süresi azalmıştır. Ayrıca, hava giriş hızının yükseltilmesinin entropi üretimini arttırdığı gözlemlenmiştir.

Anahtar Kelimeler: İçe doğru erime, küresel kapsüller, etkin ısıl iletkenlik, faz değişim malzemeleri

CONTENTS

LIST OF FIGURES

Page

LIST OF TABLES

Page

CHAPTER ONE
INTRODUCTION

This thesis consists of experimental and numerical studies on the inward melting problem inside spherical capsules. In the section of numerical studies, the influences of inlet temperature, velocity of the heat transfer fluid (HTF) and the capsule material on the performance of a latent heat thermal energy storage (LHTES) system are investigated. In the section of experimental studies, the charging performances of spherical encapsulated phase change material (PCM) were obtained under different external boundary conditions. The introduction outlines numerical and experimental studies in the literature for melting inside spherical capsules.

1.1 Thermal Energy Storage Techniques

Nowadays, energy demand arises due to the increasing population. The gap between energy production and consumption grows rapidly. Therefore it becomes more and more important to utilize current energy resources efficiently. Thermal energy storage attracts increasing interest in thermal applications. When there is a mismatch between energy storage and energy consumption, energy storage applications are required (Regin, Solanki & Saini, 2008).

Many of the renewable energy sources, such as solar and wind, are highly variable. Therefore, the energy produced by these sources can show significant fluctuations season by season, day by day. The situation may give rise to the produced energy not to coincide completely with the overall energy demand. In this respect, energy storage units are of great importance to meet the energy demand of the load in every situation (Hasnain, 1998). The excess energy that is produced from the alternative energy sources is transferred to various energy storage techniques, and this reserved energy is consumed to meet the request of the load when the primary energy sources are not adequate or inadequate. Renewable solar energy, do not provide a continuous source of energy. By storing solar energy with thermal energy storage (TES), the discrepancy between energy demand and supply would be eliminated (Regin et al., 2008).

In TES systems, the energy is stored in the period when the thermal energy source is accessible, and in the absence of energy source, the stored energy is used. By using TES systems integrated into energy systems such as renewable energy sources, a more effective and efficient use of natural resources can be ensured. For example, thermal energy that is harnessed from the solar energy can be stored day time to maintain the solar-powered heating, cooling or power production during night. The amount of energy stored in the TES systems is directly related to the internal energy variation of the storage material (Hasnain, 1998). The major way of TES techniques are: *sensible*, *latent* and *thermochemical* (Cardenas & Leon, 2013). In the sensible heat TES method, the storage of energy is achieved by the temperature increase of the storage material. Besides, in the latent heat TES method energy is stored using the phase change of the material (Regin et al., 2008). LHTES is one of the most suitable thermal energy storage methods to achieve maximum utilization of hot water from solar energy and space heating as it can store thermal energy with small temperature variations and in lower volumes (Iten & Liu, 2014). In latent heat TES systems (LHTES), a much smaller volume of higher energy can be stored compared to the sensible TES systems. The storage materials used in these systems are known as a PCM because they change phase during the process (Sarı & Karaipekli, 2007). The PCMs may undergo liquid-gas or solid-liquid phase change. However, as the liquid-gas phase change requires a storage tank that is resistant to high-pressure change, its use is limited. Besides, the solid-liquid phase change has an extensive range of practice in the energy storage or transfer with small volume differences (Hasnain, 1998).

PCMs that are used in the LHTES systems can be categorized as inorganic, organic and eutectic. The most preferred PCMs are the organic ones due to their advantages. Mostly used organic PCMs are paraffins and fatty acids. Paraffins are chemically stable throughout and after the phase change (even after 2000 cycles), long-lasting, corrosive and non-toxic. Also, they are widely used because they are easily accessible type of PCM. The paraffins have high latent heat value in phase change process. (Khadiran, Hussein, Zainal & Rusli, 2016; Rathod & Banerjee, 2013; Iten & Liu, 2014).

1.2 Literature Review

The current thesis consists of two parts as experimental and numerical. In this context, the literature review is categorized into experimental and numerical studies. In the literature, melting studies in spherical capsules were examined into experimental investigations. In addition to this, studies that are covering the modelling of single and multiple spherical capsules in TES are summarized.

1.2.1 Experimental Studies

Tan (2008) conducted several experiments for the melting process for both unconstrained and constrained melting inside a sphere using PCM. The experiments were carried out to understand how n-octadecane acts at various wall temperatures of 35°C, 40°C and 45°C with a subcooling of 1°C for unconstrained melting. Moreover, various preliminary sub-cooling temperatures of 1°C, 10°C and 20°C at a stable wall temperature of 40°C are investigated for the constrained melting. Time-dependent alteration of the liquid phase and temperature readings at various positions in the PCM were compared for two types of melting. Heat transfer mechanisms were discussed in detail for the constrained and unconstrained melting modes. Ettouney, El-Dessouky & Al-Ali (2005) concerned with the experimental evaluation of the heat transfer of the paraffin wax, which is stored inside of the spherical shells, during the energy storage and release. The results show that the Nusselt number during the melting process strongly depends on the sphere diameter, and the air velocity and air temperature have a weak influence. Chan & Tan (2006) investigated the PCM's solidification inside a spherical capsule under stable surface temperature condition. The impact of preliminary liquid superheat of the PCM has no important effect compared to the solidified mass fraction obtained at the constant surface temperature. Using paraffin wax, the heat transfer performance belongs to a spherical capsule which is analyzed by (Regin, Solanki & Saini, 2006), is located in a convective domain during the melting period. The study of (Regin et al., 2006) searched the impacts of the capsule radius on the Stefan number on the thermal performance which means the instant heat flow, the molten fraction and the time required for complete melting. Assis, Katsman, Ziskind & Letan (2007) examined the melting period of PCM in a spherical geometry experimentally and numerically. The experimental results were used to confirm the numerical findings. Results showed that the temperature difference between the mean melting and the wall temperature and the diameter of the shell parameters were important for phase change process in the numerical study. Tan, Hosseinizadeh, Khodadadi & Fan (2009) studied an experimental and numerical survey during constrained melting of PCM to understand the effect of buoyancy-driven convection in a spherical capsule. It was examined that PCM in the sphere's top region melts more faster than PCM in the sphere's bottom region. The calculation confirmed the findings of the experimental studies. Khot, Sane & Gawali (2011) studied different conditions that occur between constrained and the paraffin wax's unconstrained melting, under steady surface temperature boundary terms, various initial sub-cooling terms. Li, Wang & Kong (2015) experimentally studied the solidification and melting periods and the effect of increasing thermal conductivity of the PCM inside a spherical capsule on the phase change process of the PCM. The results show that the PCM at the top of the sphere melts quicker than the bottom and that the PCM near the inner wall solidifies quicker than the sphere's center. To quantify the heat transfer in the time being of the inward solidification of a PCM enclosed in spherical capsules, Liu et al. (2016) developed a test method during solidification based on the instant volume shrinkage of the PCM.

1.2.2 Numerical Studies

Cho & Choi (2000) examined the thermal speciality of paraffin in a spherical capsule during solidification and melting periods. They varied various parameters such as the inlet temperature during the solidification period, the preliminary temperature throughout the melting period and the Reynolds number. Ismail & Henriquez (2002) developed a numerical model to examine a storage system consisting of PCM-filled spherical capsules in a cylindrical tank. The influences of the geometrical and operational parameters on the charging and discharging of the system were examined. Bellan et al. (2015) experimentally and numerically analyzed the thermal performance of a high temperature LHTES filled with spherical capsules. This study was performed to understand the effect of different operating parameters.

Karthikeyan & Velraj (2012) presented a relative work of different mathematical domains for the LHTES system, consisting of a cylindrical storage tank which is filled with paraffin encapsulated spherical capsules. A mathematical domain is developed to examine the thermal success rate of the LHTES in regard of geometrical parameters. Karthikeyan, Solomon, Kumaresan & Velraj (2014) conducted parametric analyses on the success rate of a storage unit with PCM encapsulated spherical capsules, which is available for solar heating practises. Archibold et al. (2014) formed a spherical LHTES model and studied heat transfer and fluid flow during the melting period of a two-dimensional axisymmetric model in the sphere. Hariharan, Kumar, Kumaresan & Velraj (2018) experimentally and numerically examined the melting and solidification behaviour of the PCM, paraffin, encapsulated in a spherical container. Computational Fluid Dynamics (CFD) analyses are approved against experimental results. An LHTES mathematical model based on encapsulated PCMs is developed (Raul, Jain, Gaikwad & Saha, 2018).

The mathematical approach that is used to consider the natural convection inside capsules is an important issue to achieve reasonable findings while modeling a TES tank. The phase change problem with natural convection requires quite lower time-step sizes, *e.g.,* 0.1 s or below, to reduce the residuals of the governing equations.

However, it will be a time-consuming process to follow such a method to carry out an engineering optimization for long-term charging and discharging periods. Instead, researchers either neglect the natural convection to reduce the computational cost (Wu & Fang, 2011; Jian-you, 2008; Tao, He & Qu, 2012; Tao, He, Cui & Lin, 2013) or implement the enhanced thermal conductivity approach (Farid, Kım, Honda & Kanzawa, 1989; Adine & Qarnia, 2009; Tao & He, 2011; Bechiri & Mansouri, 2015) to take into account the influence of natural convection and increase the accuracy of the mathematical model. Scanlan, Bishop & Powe (1970) described an experimental study on natural convection between two isothermal concentric spheres. This study reported the results of the free convection among isothermal concentrically spheres. It was found that the heat transfer consequences for combined data could be simply derived in terms of k_{eff}/k and Rayleigh number.

Ezan, Uzun & Erek (2014) described the effective thermal conductivity for inward melting problems in spherical capsules with respect to temperature difference and distance between interface and shell. Regin et al. (2006) analyzed the performance of heat transfer of a spherical capsule by using paraffin wax throughout the melting period. Effective thermal conductivity is used for modeling natural convection. In the melting period, firstly the active energy transfer mode is the conduction. As the melted region grows, the importance of natural convection increases. Regin et al. (2006) solved this by combining the conduction as an active energy transfer method and by combining the free convection effect using the concept of enhanced thermal conductivity. Amin, Bruno & Belusko (2014) represented an empirical correlation to the inward melting of water in a sphere. The proposed correlation is based on the results of four representative experiments. It is stated that the correlation gives the mean value of the enhanced thermal conductivity rather than an instantaneous heat during the melting process. The constrained melting period of PCM in spherical capsule was analyzed by the model including verified natural convection. The melting periods are simulated by the conduction-controlled model with the current active thermal conductivity correlations mentioned in the literature (Liao et al., 2018).

In the thesis, firstly the phase change phenomenon inside a spherical capsule was examined numerically and experimentally. The temperature changes in the capsule and the results of the change in the heat transfer rate were obtained in the experimental study. While the single capsule was modeled numerically, enhanced thermal conductivity approach was applied. In numerical studies, change of the liquid fraction and the temperature of the capsule were investigated.

According to the literature review, the phase change phenomenon inside spherical capsules is investigated either neglecting the buoyancy effects or implementing the enhanced thermal conductivity for large-scale LHTES unit. The natural-convection-driven phase change may produce a significant impact during the melting process, and the natural convection should be taken into account in the numerical studies. The main aim of this thesis is to improve a novel script in ANSYS-FLUENT software to implement the enhanced thermal conductivity approach for the inward melting process of PCMs inside in-line arranged spherical capsules that are subjected to crossflow. Hydrodynamic characteristics, the time-wise variations of the temperatures, the heat transfer rates and rate of entropy generations are evaluated by varying the capsule material, the inlet temperature and velocity of the HTF.

CHAPTER TWO
EXPERIMENTAL INVESTIGATION

In this study, the charging performance of a TES unit that includes spherical encapsulated PCMs were obtained experimentally under various external boundary conditions. Paraffin was used as the PCM and air was used as heat transfer fluid in the study. As the charging performance of spherical encapsulated PCM is achieved, the entry velocity to the HTF test zone is kept constant, and the entry temperature is changed.

2.1 Material and Method

2.1.1 Characterization of PCM

In experimental studies, commercial paraffin wax was used as PCM. The thermal characterization analysis of PCM was implemented by using Differential Scanning Calorimetry (DSC) device, Perkin Elmer Diamond DSC with Pyris 7.0 software, to determine the melting temperature and latent heat of fusion of the material. 6 mg paraffin sample was placed in the oven with an aluminium capsule. The experiments were carried out under nitrogen atmosphere. The sample was started from 0°C to 100°C at a heating rate of 10°C/min and the sample was kept at 100°C for 1 minute. The sample was then cooled to 0°C with a cooling rate of 10°C/min. The results of heating and cooling cycles are shown in Figure 2.1.

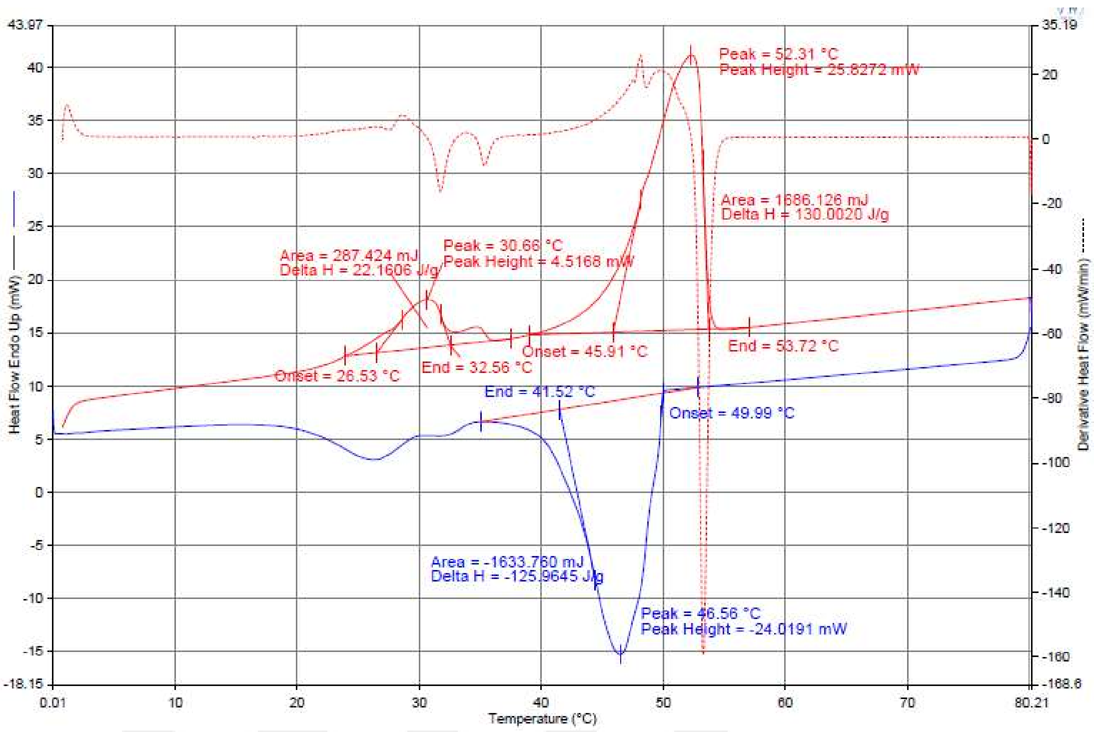

Figure 2.1 DSC thermograms for paraffin sample (heating cycle-red line and cooling cycle-blue line)

During the melting process, two endothermic peaks are observed between 26.53°C - 32.56°C and 45.91°C - 53.72°C. The first is relatively small and has probably been observed due to the impurities in the commercial material. The other peak meets the melting range of the material. The area under the curve of heat flux is calculated to evaluate the latent heat of fusion of the material. Similarly, two exothermic peaks are formed throughout the solidification period. The solidification range was obtained as 49.99°C - 41.52°C. The latent heat values for melting and solidification processes were calculated as 130.0 kJ/kg and 125.96 kJ/kg, respectively. The characteristics of the commercial paraffin are ensured in Table 2.1.

Table 2.1 Phase change characteristic of paraffin

Process	**Temperature range** (°C)	**Latent heat** (kJ/kg)
Melting	45.91 - 53.72	130.0
Solidification	49.99 - 41.52	125.96

2.1.2 Experimental Setup

In Figure 2.2 is shown the schematic diagram of the experimental set-up. The test set-up consists of a spherical capsule (4), a fixed-speed fan (1), a total of 23 T-type thermocouples for determining the mean temperatures at the inlet and outlet of the test cell, four thermocouples within the spherical capsule, and an Agilent data acquisition unit for collecting temperatures from the test cell. The results are collected within a computer and used for data reduction. Air, which is the heat transfer fluid entering the test cell, is conditioned to the temperatures above 20°C, 30°C and 35°C of the melting the PCM with the aid of a heater. The volume flow rate is calculated by pressure difference which is obtained from the differential pressure sensors located at the air inlet and outlet of the nozzle. The air is conditioned by the radial fan and heated by the electric heater until the desired temperature is reached to provide sensible heat. The temperature control of the air is carried out with the help of the thermostat in the system, and the heating process continues until the desired value is reached with the help of a controller. In order to provide a uniform velocity field at the upstream of the spheres flow straighteners are used before the inlet section of the test section.

PT-100 type temperature sensor is used to measure the input and output temperatures to the HTF test zone. T-type thermocouples were placed at various locations within the capsule to measure the time-dependent temperature changes of the PCM in the spherical capsule. The thermostats adjust the heaters to provide HTF conditioning. During the test, a maximum ± 3°C difference is provided to the test zone. In experimental studies, a photographic technique was used to observe the interface position. The thermal properties of PCM were determined by DSC.

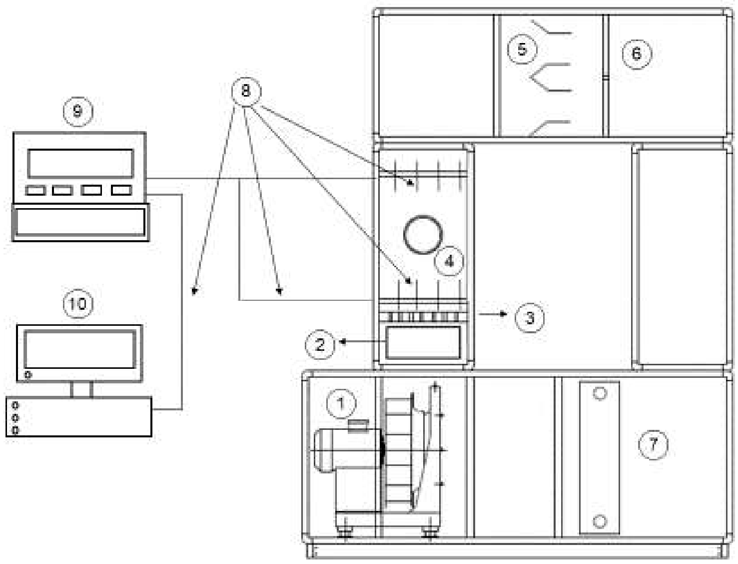

(1) Radial Fan, (2) Electric Heater, (3) Flow Straighteners, (4) Spherical Capsule, (5) Nozzle, (6) Perforated Sheet, (7) Cooling Coil, (8) Thermocouples, (9) Data Logger, (10) Computer

Figure 2.2 Schematic diagram of the experimental setup

Figure 2.3 shows a close-look to the spherical capsule. Four thermocouples are placed inside the PCM and the distance between each thermocouple is determined as 20 mm. During the test period, data, which are collected from the thermocouples, are recorded using data acquisition unit. A total of 13 thermocouples were positioned at the outlet and inlet sections of the test cell. Seven of these thermocouples are at the entrance of the test cell, and six of them are at the outlet of the test cell. The temperature variation among the inlet and outlet sections of the test cell is used to figure out the rate of heat transfer among air and PCM.

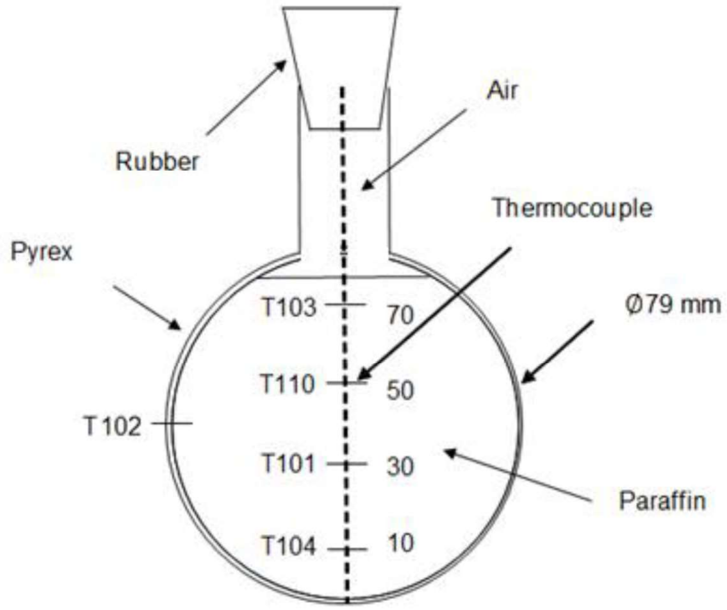

Figure 2.3 Thermocouples in the spherical capsule

2.1.3 Data Reduction

Time-wise changes of the mass flow rate, which calculated using the volumetric flow rate, and the velocity of the fluid can be seen in Figure 2.4. The range and unit of the pressure value read from the differential pressure sensor are set as desired. When the mass flow rate is calculated by applying the variable density with the help of the nozzle in the experimental setup, the pressure drop is firstly calculated and then the volume flow rate is calculated. The change in the mass flow rate in Figure 2.4 is due to the change in pressure of the fluid used in calculating the volume flow and changes in the inlet temperature of the test cell.

In Figure 2.4, the Equation (2.1) and Equation (2.2) were used to reach the time dependent change graph of the mass flow changes based on the experimentally studied temperature values. The differential pressure sensor connected to the nozzle in the test device reads the pressure drop. This value is applied to the Bernoulli equation in Equation (2.1) and the mass conservation equation for nozzle in Equation (2.2) and the volumetric flow rate is calculated using Equations (2.3), (2.4) and (2.5).

Then, the mass flow rate was reached with varying density value depending on the temperature. Equation (2.5) is obtained using Equation (2.1) and Equation (2.2).

$$\frac{P_1}{\rho g} + \frac{V_1^2}{2g} + z_1 = \frac{P_2}{\rho g} + \frac{V_2^2}{2g} + z_2 \tag{2.1}$$

$$V_1 A_1 = V_2 A_2 \tag{2.2}$$

Equation (2.3), ΔP shows the pressure drop, ρ density, R universal gas constant.

$$\alpha = -(\frac{\Delta P}{\rho_{air} R_{air} T_{air}}) \tag{2.3}$$

The coefficient found in Equation (2.3) was used to find the Y coefficient in equation (2.4). Then the Y value in equation (2.5) allows us to calculate the volumetric flow rate.

$$Y = 1 - 0.548(1 - \alpha) \tag{2.4}$$

$$Q = Y\sqrt{\frac{2\Delta P}{\rho_{air}}} \sum CA \tag{2.5}$$

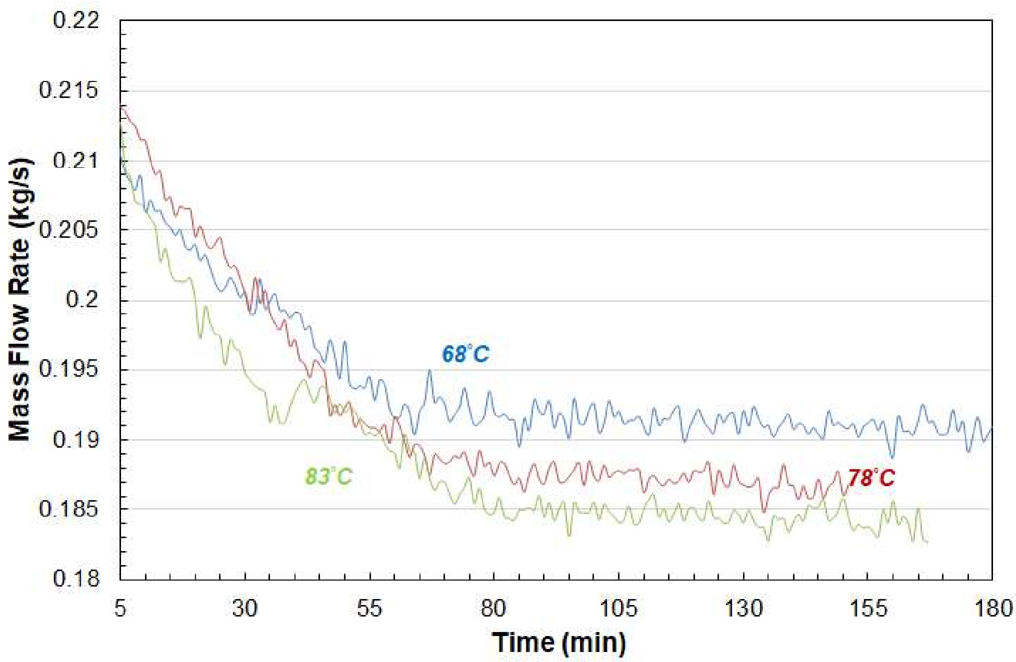

Figure 2.4 Time-dependent change of mass flow rate of air for T_{set} = 68°C, T_{set} = 78°C and T_{set} = 83°C

The experiments were carried out to observe the changes in PCM's melting. The obtained results were interpreted by means of variable density approach of mass flow of air, the temperature change in capsule and temperature changes of fluid entering and leaving the test cell. The experiments were executed at temperatures of 68°C, 78°C and 83°C. In experiments, it is observed that as the difference between the phase change temperature and the outdoor temperature increased, there was a progress in the heat transfer rate and decrement in the storage time. Due to the temperature-dependent variation of thermophysical properties such as viscosity and density, a difference of 3% is formed between the mass flow rates at the set values.

Figure 2.5 shows the time-dependent difference of the heat transfer rate. The heat transfer rate between the HTF and PCM was calculated using Equation 2.6. Also, in Equation 2.6, the temperature difference was calculated by using the temperature of the fluid when it is entering and leaving the test cell.

$$\dot{Q} = \dot{m}c_p(T_{in} - T_{out}) \tag{2.6}$$

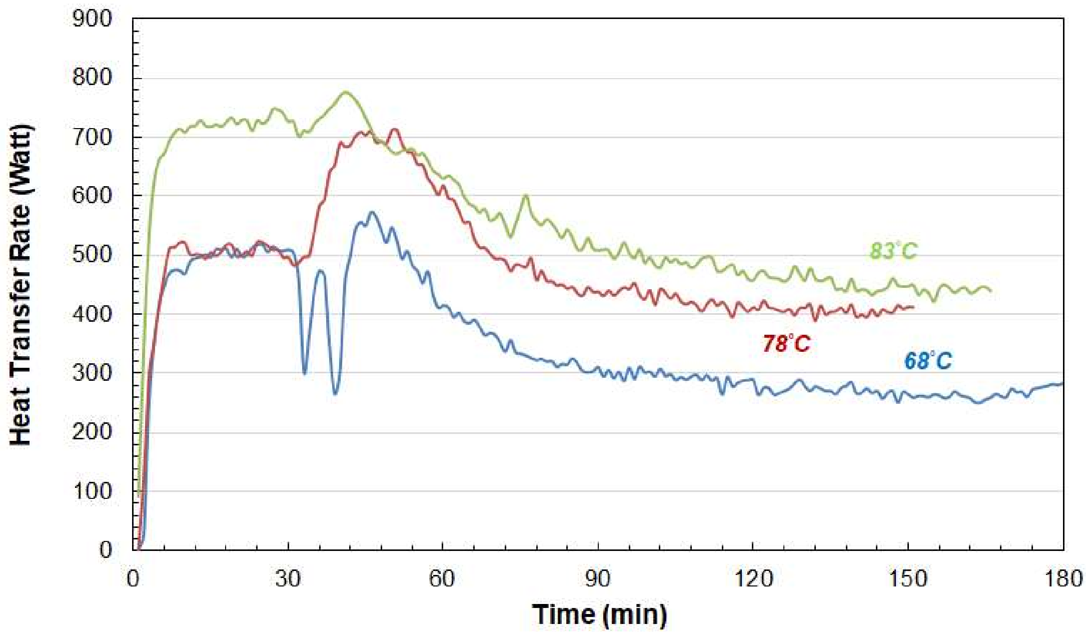

Figure 2.5 Time-dependent change of heat transfer rate of air for T_{set} = 68°C, T_{set} = 78°C and T_{set} = 83°C

2.2 Experimental Results

Experiments are initiated at nearly 25°C, and the inlet temperature of the fluid to the test cell was set at 68°C, 78°C and 83°C. The temperature variations inside the spherical capsule are shown in Figure 2.6, Figure 2.7 and Figure 2.8 for the inlet temperature of 68°C, 78°C and 83°C, respectively. When the temperature reaches the phase change temperature of the paraffin, the slopes of the curves suddenly changes and the rate of temperature changes slows down due to the internal energy variation within the PCM via latent heat in Figure 2.6. It is interesting to note that the temperature at the upper part of the sphere *i.e.,* $T_{1,}$ increases more quickly when it is compared with the bottom region. At the upper part of the sphere, a small air gap is intentionally left for compensating volume change of the PCM. At the upper region of the capsule temperature of air increases more rapidly than the PCM, due to small thermal mass of air, and this increment results enhancement in heat transfer rate. The temperature of the thermocouple at the top of the sphere *i.e.*, $T_{1,}$ reaches to the phase change temperature of PCM approximately in 40 min. Besides, for the bottom one, it takes more than 120 min to reach the melting temperature. Results reveal that the melting starts from top side of the sphere and it advances to bottom part of the sphere. The thermocouples which are indicated as T_2 and T_3 reach to melting zone nearly 60 min and 110 min, respectively. Moreover, the inlet temperature of the HTF, $T_{entrance}$, varies at the early periods of the experiment, due to the storage capacity of the PCM sphere, and reaches to steady-state temperature after 60 min.

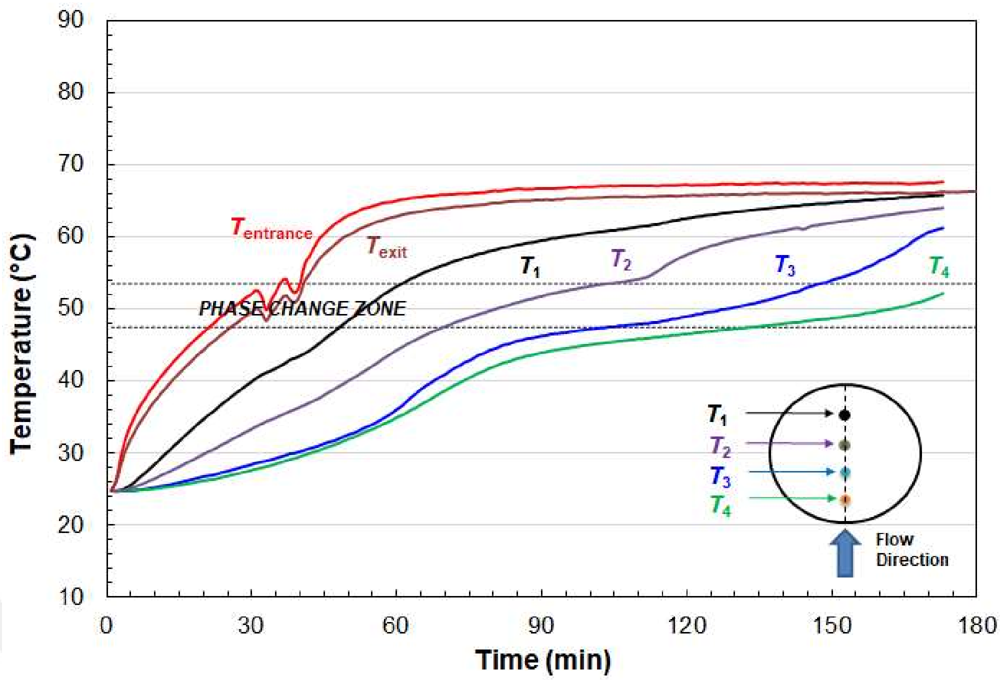

Figure 2.6 Temperature change inside the capsule for T_{set} = 68°C

The temperature change in the capsule is shown in Figure 2.7 where the HTF is taken as the inlet temperature 78°C to the test cell. In Figure 2.7, the difference in the slope of the temperature curves of the thermocouples in the phase change zone is due to the change in the heat transfer mechanisms, the transition from conduction to convection. In Figure 2.6, Figure 2.7 and Figure 2.8 can be seen after phase change region *i.e.,* at temperatures above 53.50°C, slope of the curves approach each other. When the desired set point is reached, a stable system is formed. The average of the initial temperatures is 68.5°C for the set point of 68 °C, 68.64 °C for the set point of 78 °C, and 75.18 °C for the set point of 83 °C. Higher set point temperatures, the increase in the average value of the inlet temperature of the test cell is consistent. In Figure 2.7, the thermocouples which are indicated as T_2 and T_3 reach to melting zone nearly 60 min and 90 min, respectively. Moreover, the inlet temperature of the HTF, $T_{entrance}$, reaches to steady-state temperature after 55 min.

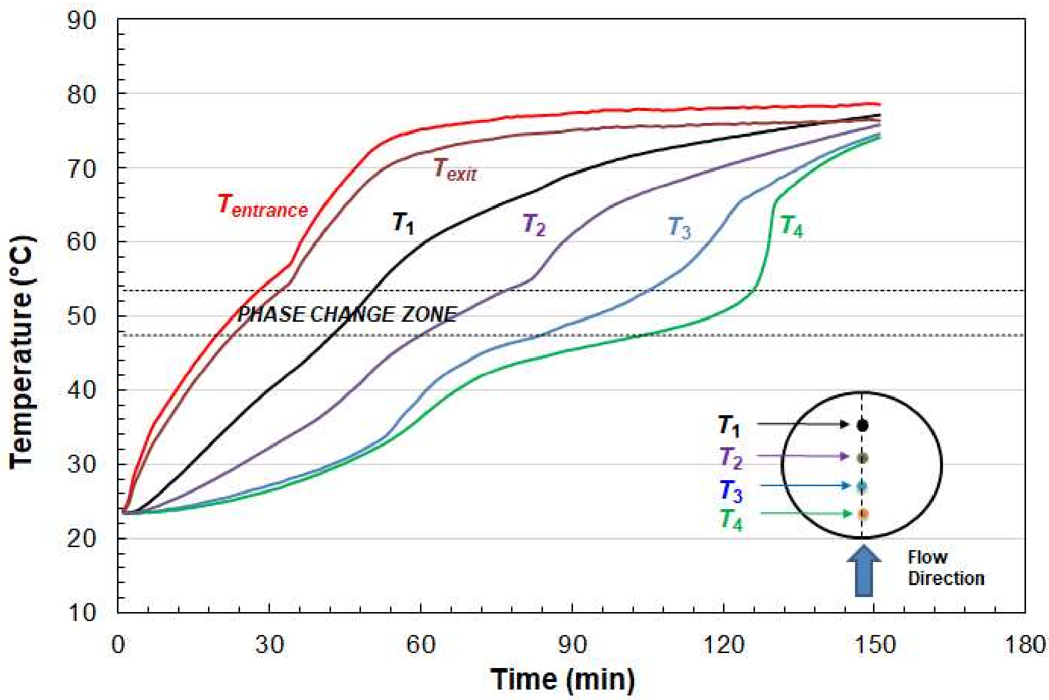

Figure 2.7 Temperature change inside capsule for T_{set} = 78°C

The temperature change in the capsule is shown in Figure 2.8 where the heat transfer fluid is taken as the inlet temperature 83°C to the test cell. Instant heat transfer of air decreases as time passes. Heat transfer is caused by the temperature difference between the paraffin and the fluid in the spherical capsule. When the paraffin is completely melted, the temperature of the circulating fluid in the system becomes stable with the temperature of the paraffin. Therefore, after the temperatures in the capsule have passed the phase change zone, the temperature curves are closer to each other and become more stable. Since inlet temperature to test cell is set to 83°C, the entrance temperature of the test cell is considerably higher than the phase change temperature range of the paraffin. So, the temperature in the capsule continues to increase even after completing the melting process in the paraffin phase change zone. This causes the variation between the entrance temperature of the fluid and the exit temperature in the test cell. In Figure 2.8, the thermocouples which are indicated as T_2 and T_3 reach to melting zone nearly 50 min and 75 min, respectively. Moreover, the inlet temperature of the HTF, $T_{entrance}$, reaches to steady-state temperature after 50 min.

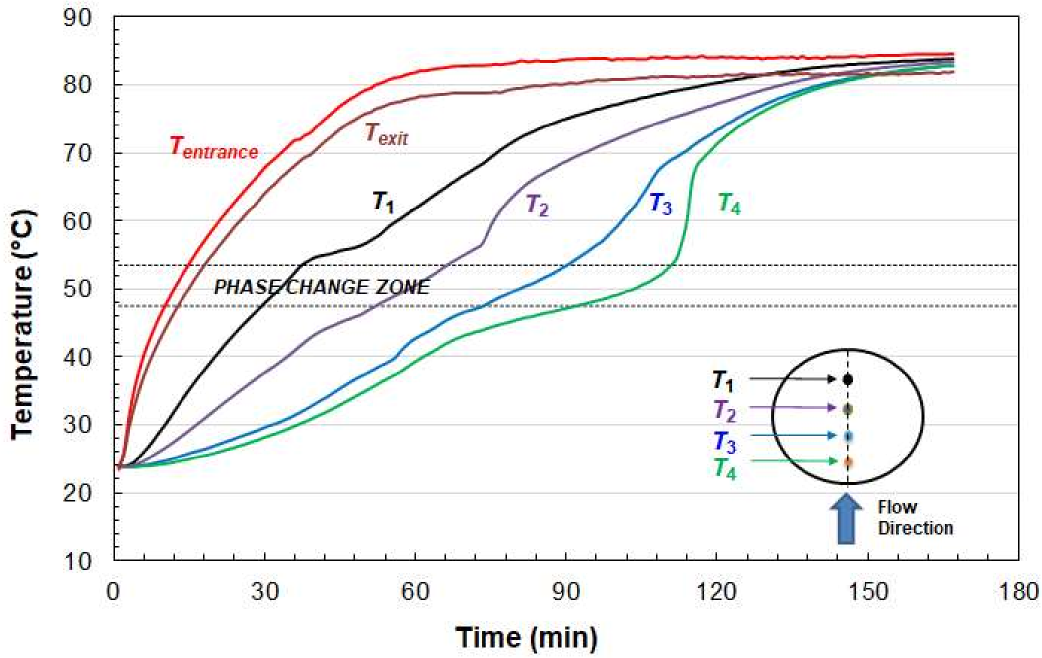

Figure 2.8 Temperature change inside the capsule for T_{set} = 83°C

Table 2.2 shows the time to attain the lower limit of the phase change temperature range of the thermocouples in the capsule in minutes. Also, here the time to reach the inlet temperature of the test cells to the set values of 68°C, 78°C and 83°C. For a set point of 68°C, the time to reach the test cell to the phase change temperature (53.5°C) is 40 minutes. The time to reach phase change temperature for 78°C and 83°C was 28 and 15 minutes, respectively. As the inlet temperature increases to the test cell, the time required to reach 53.50°C decreases. The interpretation for $T_{entrance}$ applies to the thermocouples in the capsule. For the set point T_2 of 68°C, the time to reach the test cell to the phase change temperature (53.5°C) is 104 minutes. The time to phase change temperature for 78°C and 83°C was 77 and 67 minutes, respectively. Since T_1 is in contact with air, this thermocouple reaches the phase change temperature before the others.

Table 2.2 Time required to reach complete melting (min)

T_{set}	$T_{entrance}$	T_1	T_2	T_3	T_4
68°C	40	62	104	148	176
78°C	28	51	77	105	126
83°C	15	38	67	91	111

For 83°C set temperature, the melting phase in the sphere is stated in Figure 2.9. The non-transparent white part shows solid PCM and the transparent part shows liquid PCM. Melting takes place primarily heat conduction from the capsule surface. Since the rod inside of the capsule constrains the melting, the solid PCM does not move into the bottom of the capsule as the melting progresses. Since there are natural convection effects on the upper parts, the melting is more effective in the upper regions. Even though the flow direction is through the upwards, the melting front grows through the downward direction. Air gap at the upper part of the capsule allows to increase the PCM temperature more rapidly at the top of the capsule. For 68°C set temperature, the melting phase within the sphere is stated in Figure 2.10. It is observed that there is a difference in liquid fraction when comparing the two temperatures in the same minutes. Especially after 90 minutes, the differences in liquid fraction become more apparent. Up to 90 minutes, the four thermocouples in the capsule for 83°C reached the phase change temperature. However, up to 90 minutes for 68°C, only T_1 and T_2 entered the phase change zone. T_3 and T_4 did not reach 53.50°C.

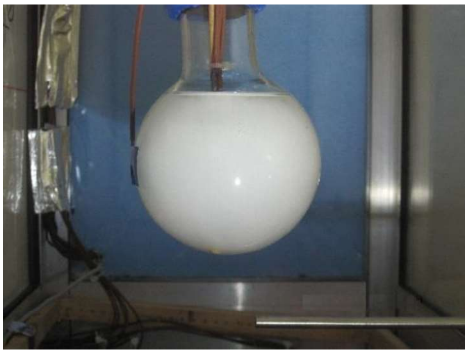

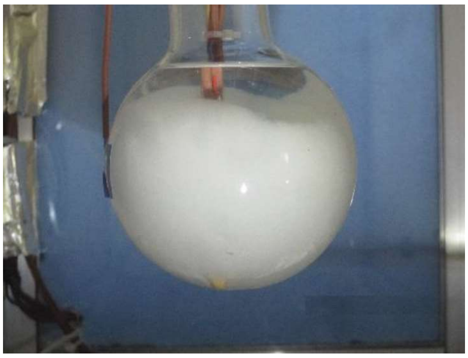

(a) 0 minute (b) 30 minutes

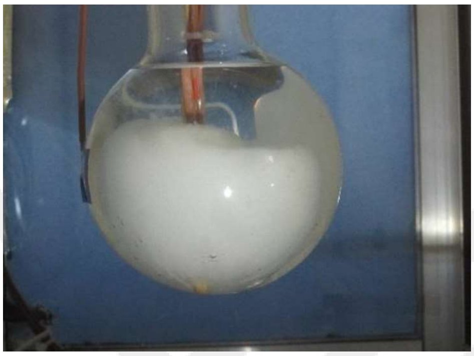

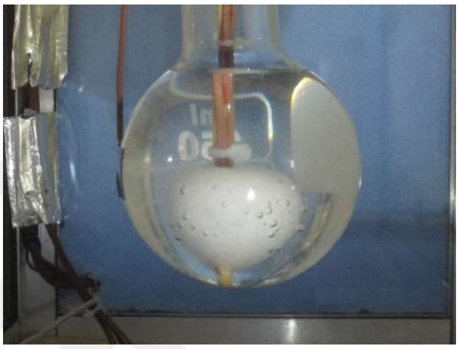

(c) 60 minutes (d) 90 minutes

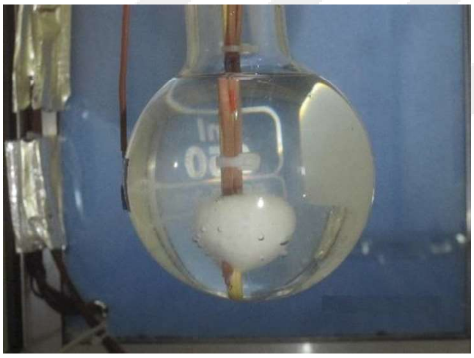

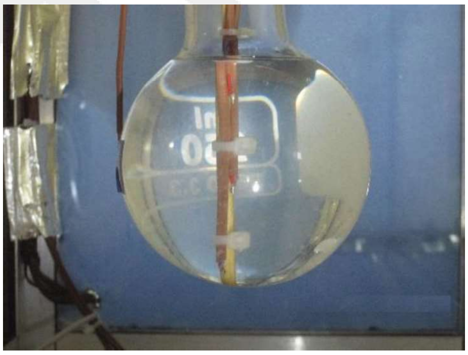

(e) 120 minutes (f) 150 minutes

Figure 2.9 Instantaneous photographs of the melting of PCM inside the spherical capsule for T_{set} = 83°C (Personal archive, 2017)

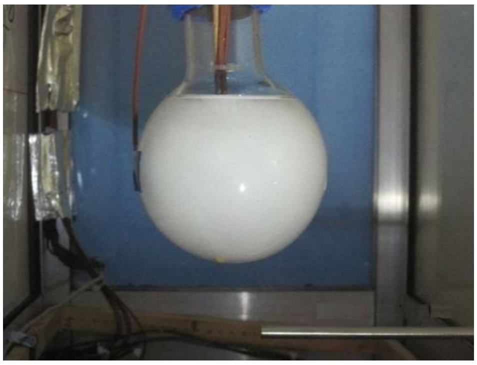

(a) 0 minute

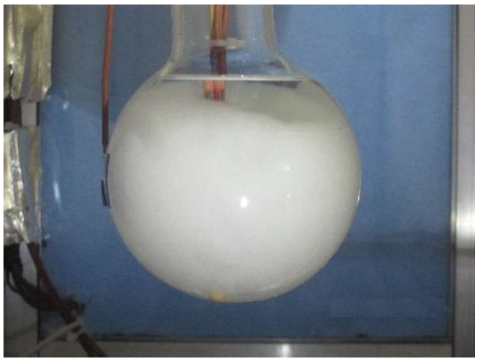

(b) 30 minutes

(c) 60 minutes

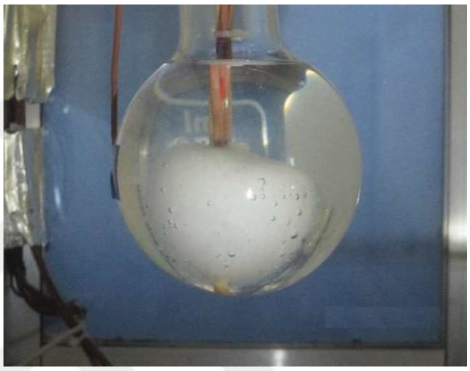

(d) 90 minutes

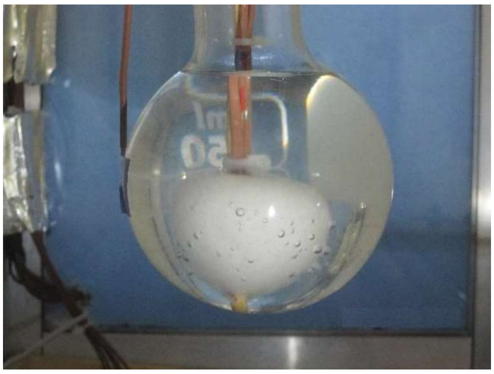

(e) 120 minutes

(f) 150 minutes

Figure 2.10 Instantaneous photographs of the melting of PCM inside the spherical capsule for T_{set} = 68°C (Personal archive, 2017)

CHAPTER THREE
NUMERICAL INVESTIGATION

The influences of inlet temperature and velocity of the HTF and the capsule material on the performance of a LHTES unit is numerically investigated. The enhanced thermal conductivity approach is implemented into the ANSYS-FLUENT software to consider the natural-convection-dominated melting process within capsules with two different configurations. The accuracy of the procedure is checked by comparing the current findings for inward melting against the numerical results from the literature. In the first set of parametric analyses, a single capsule is exposed to the forced convection and results are classed with the current experimental measurement. In the second set, on the other hand, inward melting of PCMs inside in-lined capsules are numerically investigated.

3.1 Forced Convection around a Single Capsule

3.1.1 Definition of Problem

Analyses were made to validate the studies performed in the experiment. In the ANSYS-FLUENT package program, the test cell of the test setup is modeled. Parameters such as environmental conditions, capsule diameter, capsule material, inlet conditions of heat transfer fluid into the test cell were taken as the same with the experimental study. For the three different conditions as in the experiment, the temperature of the HTF to the test cell was set to 68°C, 78°C and 83°C. The inner diameter of the sphere used is D_s = 80 mm and the wall thickness of the sphere is Δr = 2 mm. The analysis with three different inlet temperatures was carried out and the temperature values were read from four different points in the spherical capsule and compared with the experimental results. Sphere material was taken as glass. Test cell is reduced in to a 2D axisymmetric model as shown in Figure 3.1. The spherical capsule has a stem over the bulb volume. The PCM is filled inside the bulb and air spacing is left at the top of the blub to allow volume change of PCM during phase change. Rubber is attached on the stem to prevent the mass transfer from the sphere to HTF.

In Figure 3.1, the thickness of the air on the capsule is 40 mm. The air is in contact with the PCM in the spherical capsule. The thickness of the rubber on the air is 52 mm. Rubber is used to prevent air contact with the HTF outside the capsule. The distance from the center of the spherical capsule to the inlet of the computational domain is 250 mm. The distance of the rubber on the capsule to the outlet section of the computational domain is 150 mm.

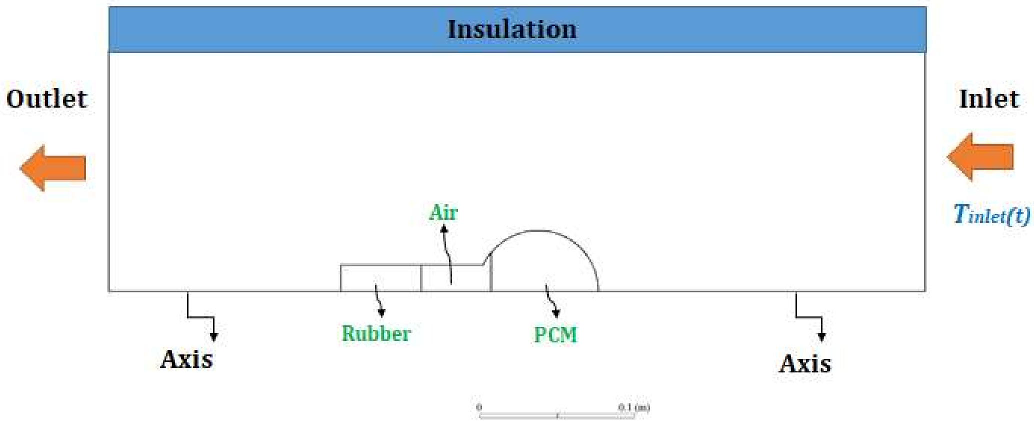

Figure 3.1 Computational domain of single sphere capsule with PCM

Table 3.1 Properties of spheres material and PCM

Property	Pyrex Glass	PCM
Thermal conductivity, W/mK	1.4	0.385 (solid) 0.1505 (liquid)
Specific heat, J/kgK	835	2330
Density, kg/m^3	2225	772
Kinematic viscosity, m^2/s	-	5E-6
Latent heat of fusion, kJ/kg	-	243.5
Thermal expansion coefficient, K^{-1}	-	0.00091
Reference	Cengel & Ghajar (2015)	Tan et al. (2009)

3.1.2 Governing Equations

In the numerical model, the following assumptions are considered,

- Working fluids are incompressible and Newtonian,
- The flow-field is fully turbulent, 2D and axisymmetric,
- While the thermophysical properties of PCM and air remain constant, it is assumed that the thermal conductivity of the liquid PCM changes,
- The thermal conductivity of PCM in the liquid phase is evaluated by using the enhanced thermal conductivity approach,

For a transient heat transfer problem inside an axisymmetric and 2D geometry, the governing equations for fluid flow domain reduce in the following form (ANSYS-Fluent Theory Guide, n.d.)

for mass:

$$\frac{\partial}{\partial x}\left(v_x\right)+\frac{1}{r}\frac{\partial}{\partial r}\left(rv_r\right)=0 \tag{3.1}$$

for x-momentum:

$$\begin{aligned}\frac{\partial}{\partial t}\left(v_x\right)+\frac{1}{r}\frac{\partial}{\partial x}\left(rv_xv_x\right)+\frac{1}{r}\frac{\partial}{\partial r}\left(rv_rv_x\right)=-\frac{1}{\rho}\frac{\partial p}{\partial x}+\frac{1}{r}\left(\frac{\mu+\mu_t}{\rho}\right)\frac{\partial}{\partial x}\left[r\left(2\frac{\partial v_x}{\partial x}-\frac{2}{3}\left(\nabla\cdot\vec{v}\right)\right)\right]\\+\frac{1}{r}\left(\frac{\mu+\mu_t}{\rho}\right)\frac{\partial}{\partial r}\left[r\left(\frac{\partial v_x}{\partial r}+\frac{\partial v_r}{\partial x}\right)\right]\end{aligned} \tag{3.2}$$

for r-momentum:

$$\begin{aligned}\frac{\partial}{\partial t}\left(v_r\right)+\frac{1}{r}\frac{\partial}{\partial x}\left(rv_xv_r\right)+\frac{1}{r}\frac{\partial}{\partial r}\left(rv_rv_r\right)=-\frac{1}{\rho}\frac{\partial p}{\partial r}+\frac{1}{r}\left(\frac{\mu+\mu_t}{\rho}\right)\frac{\partial}{\partial x}\left[r\left(\frac{\partial v_r}{\partial x}+\frac{\partial v_x}{\partial r}\right)\right]\\+\frac{1}{r}\left(\frac{\mu+\mu_t}{\rho}\right)\frac{\partial}{\partial r}\left[r\left(2\frac{\partial v_r}{\partial r}-\frac{2}{3}\left(\nabla\cdot\vec{v}\right)\right)\right]\\+\left(\frac{\mu+\mu_t}{\rho}\right)\left[\frac{2}{3r}\left(\nabla\cdot\vec{v}\right)-2\frac{v_r}{r^2}\right]\end{aligned} \tag{3.3}$$

for energy:

$$\frac{\partial}{\partial t}(\rho h)+\nabla\cdot\left(\vec{v}(\rho h)\right)=\nabla\cdot\left(k_{eff}\nabla T\right) \tag{3.4}$$

where the divergence of the velocity vector is defined as

$$\nabla\cdot\vec{v}=\frac{\partial v_x}{\partial x}+\frac{\partial v_r}{\partial r}+\frac{v_r}{r} \tag{3.5}$$

k_{eff} in Equation (3.4) stands for the effective thermal conductivity of the working fluid, *i.e.,* air, and it includes the turbulent thermal conductivity. The flow Reynolds number is defined regarding the capsule diameter as $\mathrm{Re}_D=\rho U_{inlet}D_s/\mu$. For the selected inlet velocities of 0.5 m/s, 1.0 m/s and 3 m/s, the corresponding flow Reynolds are evaluated as 1.1×10^3, 2.2×10^3, and 6.6×10^3. In order to achieve a better convergence and to capture the separation bubble between each sphere, the realizable *k*-epsilon turbulence model is used (ANSYS-Fluent Theory Guide, n.d.).

For the sphere wall and PCM domains the heat conduction equation is resolved in the following form

for energy:

$$\frac{\partial}{\partial t}(\rho H)=\nabla\cdot\left(k\nabla T\right) \tag{3.6}$$

where H (in J/kg) is the total enthalpy which involves the latent and sensible heat components of the material. The enthalpy-porosity method of (Voile & Prakash, 1987) is implemented to consider the latent heat of PCM in the energy equation. The effect of free convection within the liquid phase of PCM is taken into consideration in the energy equation regarding the enhanced thermal conductivity ($k_{enhanced}$) approach. The details of this approach are explained in the following sub-section.

3.1.3 Solution Method

A commercial CFD software, ANSYS-FLUENT, is used to resolve the transient governing equations that are given in Equations (3.1) to (3.6). Initially, it is assumed that temperature distribution is uniform within the computational domain as $T(r, x, t=0) = T_{init} = 20°C$. The segregated iterative solution procedure of (Patankar, 1980) is used to compute the pressure and velocity fields. Second Order Upwind scheme is used for interpolating the transport parameters at the interfaces of each control volume. The computational domain is divided into 162588 structured computational volumes, and the grid density is increased adjacent to the no-slip surfaces. The residuals of governing equations are reduced below 10^{-8} at the end of each time-step to satisfy the convergence.

3.1.3.1 The Enhanced Thermal Conductivity Approach

In this thesis, enhanced thermal conductivity correlations are implemented into the ANSYS-FLUENT software via user-defined-functions (UDFs) to consider the effect of free convection inside the liquid phase of the PCM without resolving the flow-field equations in the liquid PCM domain. The enhanced thermal conductivity of a fluid is defined merely as

$$k_{enhanced} = k\mathrm{Nu} \tag{3.7}$$

where the thermal conductivity on the right-hand side, k, stands for the conductivity of the liquid PCM, and the Nusselt number, Nu, is for the natural convection inside the spherical annulus. Numerous Nusselt correlations are provided in the literature to evaluate the Nusselt number for the free convection inside a spherical annular gap. In Table 3.2 four different Nusselt correlations that are proposed in the recent review of are provided (Liao et al., 2018).

Table 3.2 Nusselt correlations for natural convection inside the spherical annulus

Correlation	Reference
$\mathrm{Nu}_1 = \left(3.8475\times10^{-8}\right)\mathrm{Ra}_{r_i} + 1.5859$	Tan et al. (2009)
$\mathrm{Nu}_2 = 0.18\left(\mathrm{Ra}_{r_i}\right)^{0.25}$	Chiu & Chen (1996)
$\mathrm{Nu}_3 = 0.228\left(\mathrm{Ra}_\delta \dfrac{\delta}{r_i}\right)^{0.226}$	Scanlan et al. (1970)
$\mathrm{Nu}_4 = 0.202\left(\mathrm{Ra}_\delta\right)^{0.228}\left(\dfrac{\delta}{r_i}\right)^{0.252}\mathrm{Pr}^{0.029}$	Scanlan et al. (1970)

In the current work, an idealized inward melting model is considered to detect the enhanced thermal conductivity of the liquid PCM. In Figure 3.2, the actual and idealized interface variations for the inward melting period inside a spherical capsule are represented. In the actual process, the region of liquid PCM is transformed from the concentric to eccentric shape depending on the thermal boundary condition that is defined on the wall of the sphere. In the current model, the non-uniform interface variations are reduced into an equivalent eccentric one as illustrated in Figure 3.2 (*idealized process*). The equivalent inner radii correspond to the position of the solid/liquid interface of the PCM. The equivalent gap thickness of the liquid PCM is defined regarding the equivalent interface radius (r_{eq}) as

$$\delta = r_s - r_{eq} \tag{3.8}$$

where r_s (= $D_s/2$) is the radius of the sphere. The Rayleigh number is then defined as follows

$$Ra_\delta = \frac{g\beta\delta^3(\bar{T}_{wall} - T_m)}{\vartheta\alpha} \tag{3.9}$$

where $\bar{T}_{wall}$ is the average temperature of the inner surface of the sphere wall and T_m is the melting temperature of the PCM, respectively. UDFs are coded in C programming language and incorporated into the ANSYS-FLUENT software to determine the enhanced thermal conductivity, $k_{enhanced}$ in Equation (3.7), at the end of each iteration.

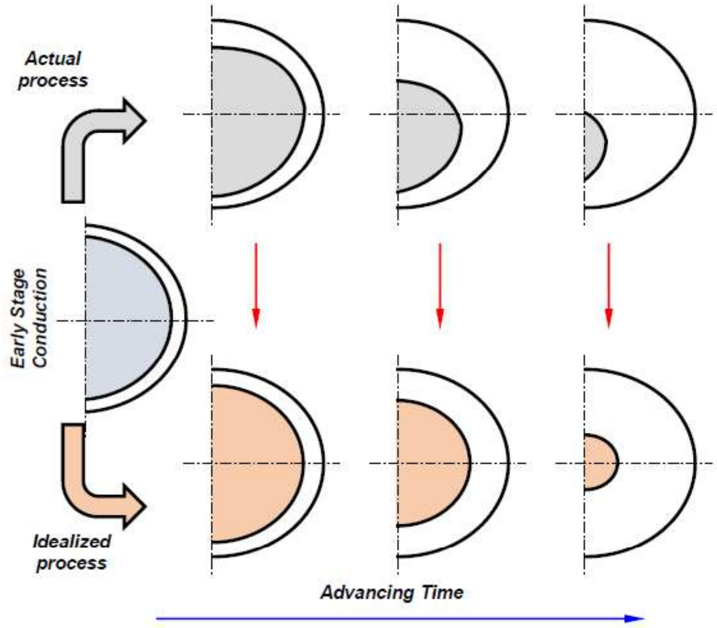

Figure 3.2 The definition of the equivalent interface position for inward melting

3.1.4 Validation of the Enhanced Thermal Conductivity Approach

Tan et al. (2009) carried out an extensive work on inward melting of *n-octadecane* in a spherical capsule. The effect of free convection on the evolution of the interface front of the PCM during constrained melting is observed both experimentally and numerically. Tan et al. (2009) used ANSYS-FLUENT software to solve the natural convection driven phase change problem. To reveal the validity of the proposed enhanced thermal conductivity approach for the inward melting inside the sphere, the work of is reproduced (Tan et al., 2009). In this study, the PCM is initially at 26.5°C, and the outer wall of the sphere is suddenly increased to 45°C and kept constant throughout the process. The time-wise variations of the liquid fractions that are evaluated for five different approaches are provided in Figure 3.3. Here the current predictions are compared with ones that are provided in the reference study. The square markers indicate the numerical results (Tan et al., 2009). The corresponding Nusselt correlations for Nu_1, Nu_2, Nu_3, and Nu_4 are given in Table 3.2. Moreover, the results of pure conduction case are also represented in the same figure. Notice that the pure conduction case is close to the variations in the reference work for the initial period of the melting process. The pure conduction case deviates from the numerical results of (Tan et al., 2009) beyond 20 min and erroneously predicts the melting process. Among the four alternatives, the Nusselt correlation, *i.e.,* Nu_4, gives the closest predictions to the time-wise variations of the liquid fraction that are provided in the reference work. That is the Nu_4 is used in the parametric results to detect the enhanced thermal conductivity of the PCM's liquid phase.

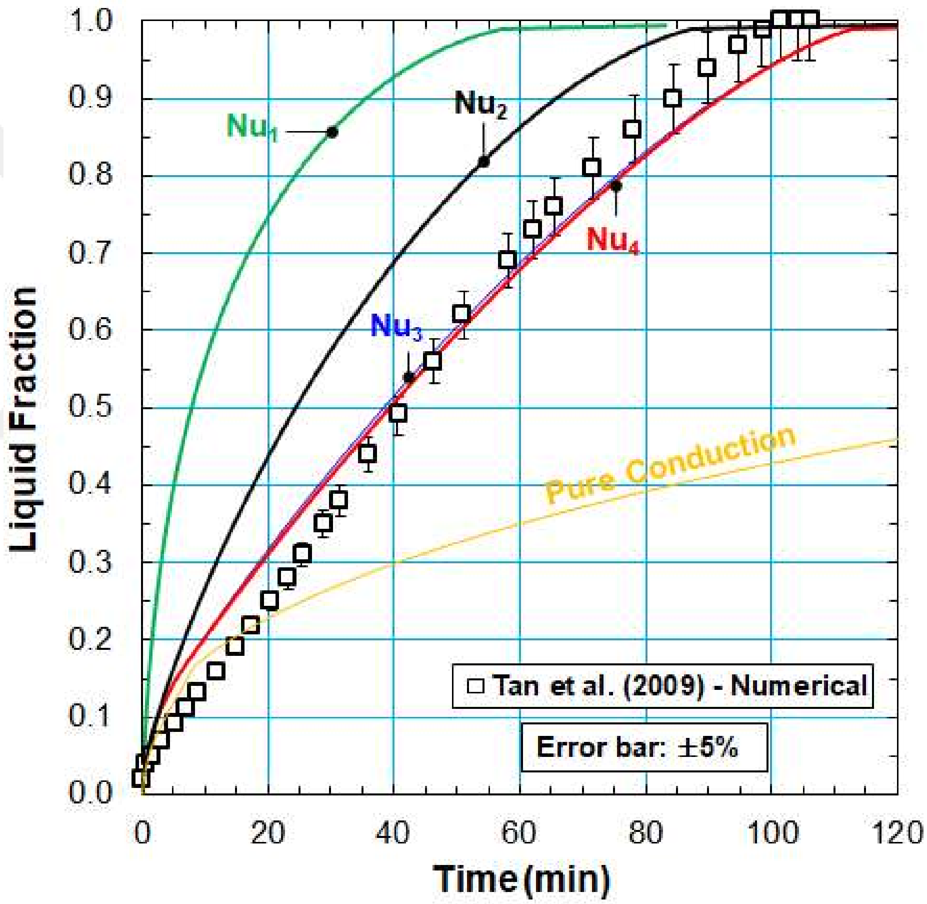

Figure 3.3 Comparison of the different correlations

3.1.5 Comparative Results of Experimental Results with Numerical Results

During the melting process, temperature distribution and liquid fraction were examined in the capsule. The capsule consists of rubber, air and paraffin. Due to the differences in thermodynamic properties, the air warms up earlier and cools earlier. If one look at the inside of the capsule within 90 minutes, the increase in the temperature of the paraffin, as expected, is 83°C, 78°C and 68°C, respectively. For 90 minutes, the liquid fraction is 83°C, 78°C and 68°C, respectively. The melting process begins at the walls of the capsule and is carried downwards from the neck. The change in temperature and liquid fraction of the capsules obtained as a result of numerical studies are given below Figure 3.4, Figure 3.5 and Figure 3.6.

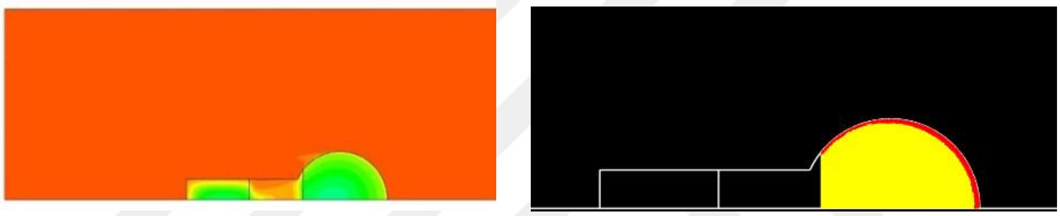

(a) t = 30 min

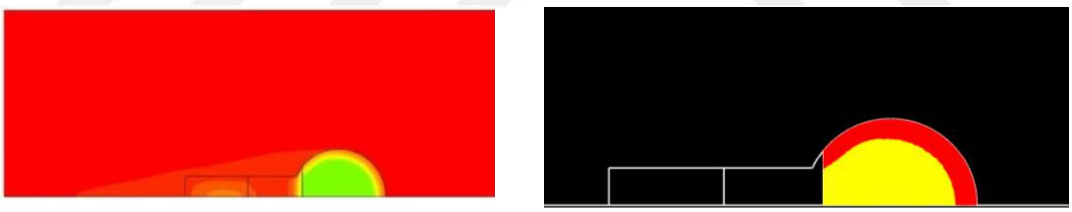

(b) t = 60 min

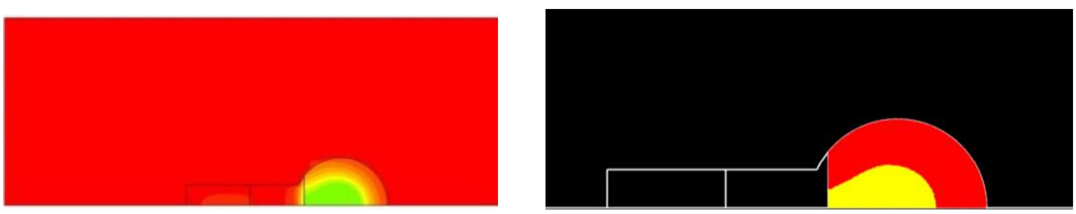

(c) t = 90 min

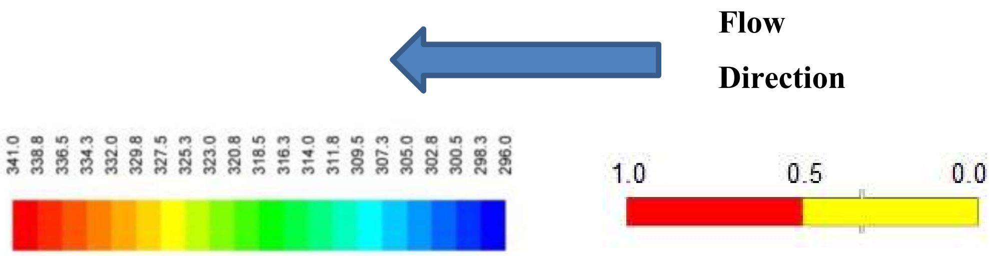

Figure 3.4 Temperature distribution and melting fraction for T_{set} = 68°C – 30, 60 and 90 minute

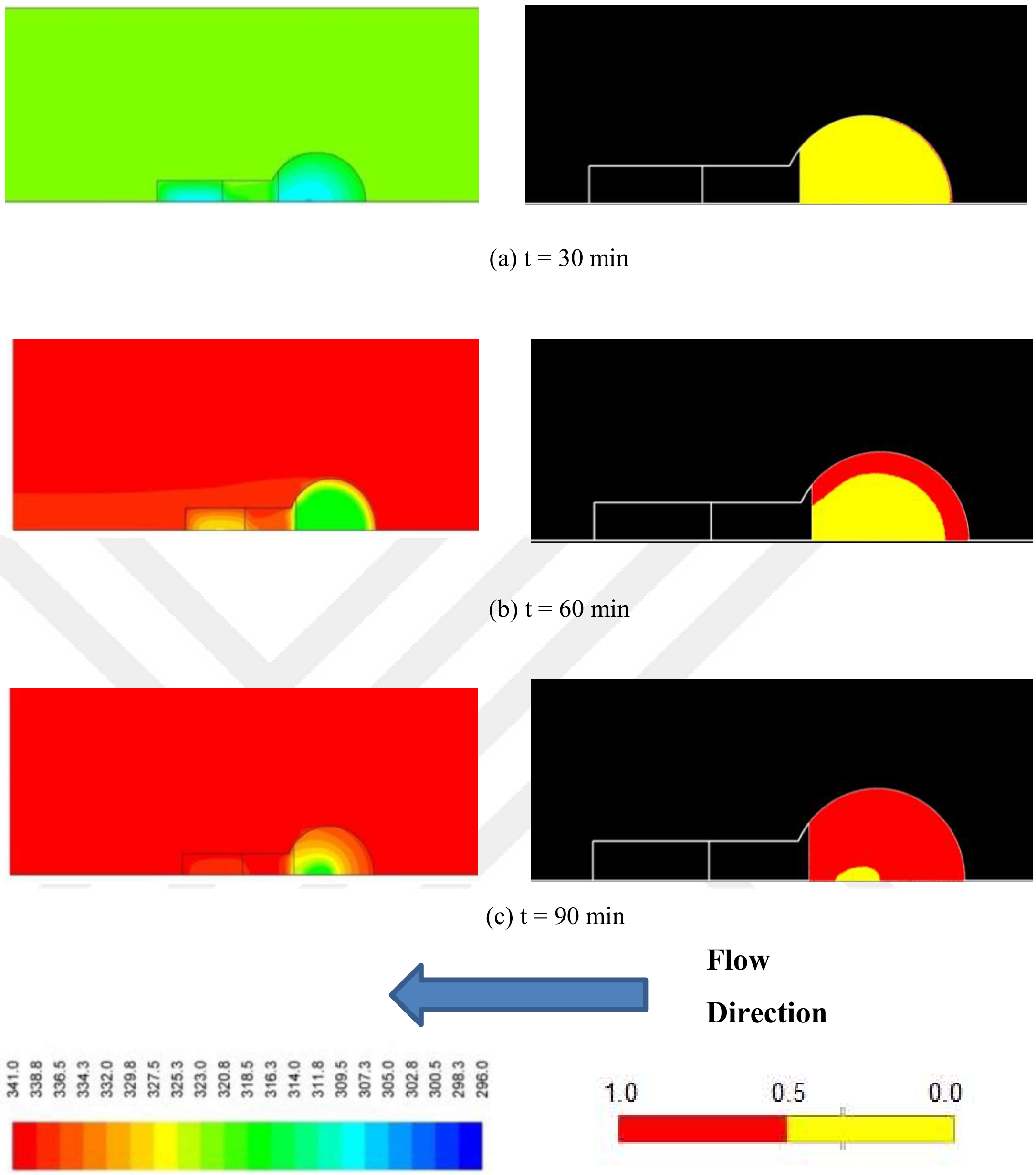

Figure 3.5 Temperature distribution and melting fraction for T_{set} = 78°C – 30, 60 and 90 minute

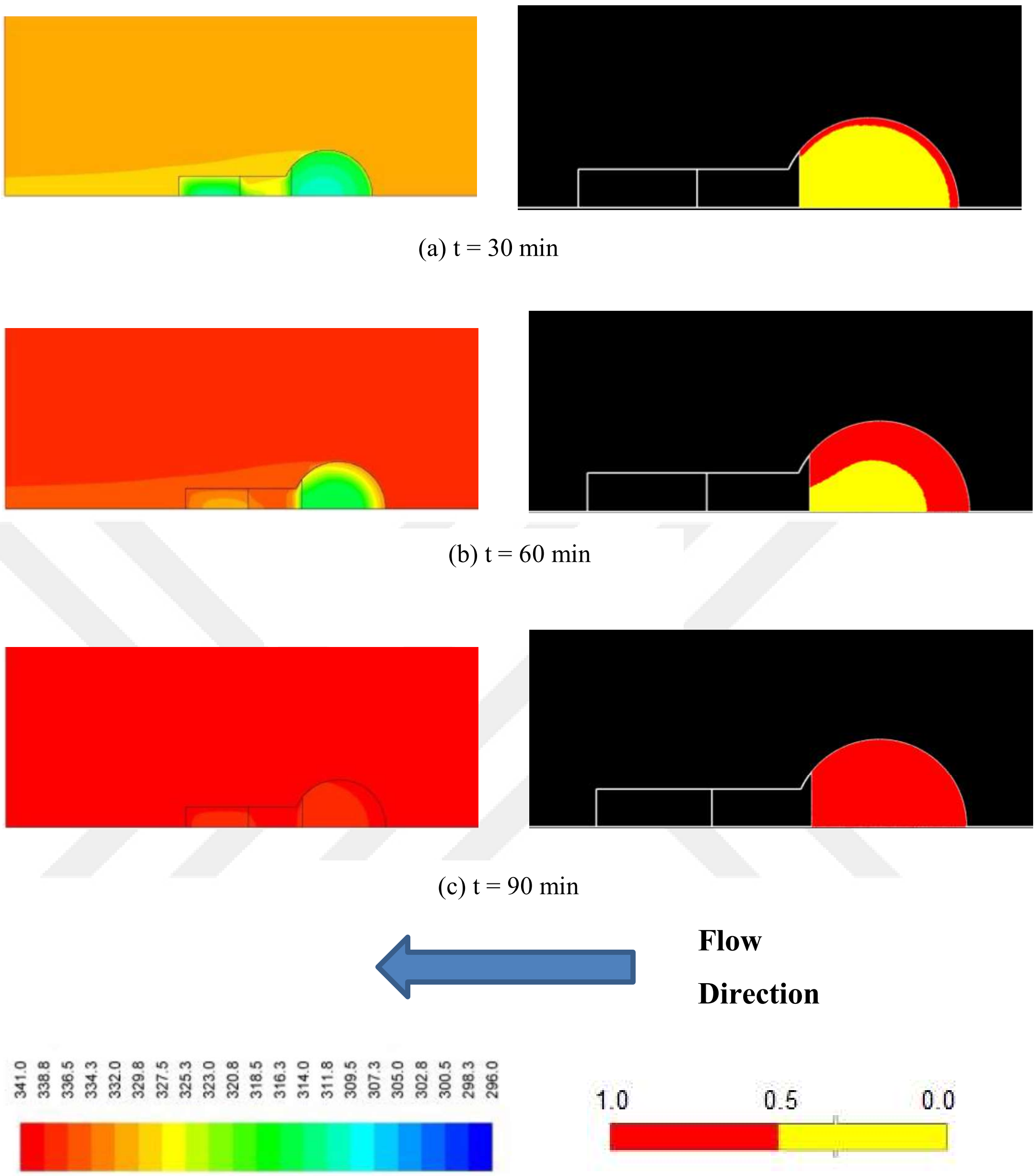

Figure 3.6 Temperature distribution and melting fraction for T_{set} = 83°C – 30, 60 and 90 minute

In the graph Figure 3.7, Figure 3.8 and Figure 3.9 where the temperature changes are observed in the capsule, when the curves formed by the numerical results are examined, a more clearly visible constant temperature condition occurs in the phase change zone contrasted to the experimental results. The T_1 curve, the thermocouple, located in the top of the sphere, is in contact with the air in the capsule. The slope of the four curves differ when the temperature curves pass through the phase change zone. The difference in the slope of the phase change zone is due to the change in the heat transfer mechanisms, the transition from conduction to convection. In the graph Figure 3.7, Figure 3.8 and Figure 3.9, dashed lines show numerical results. Others show experimental results.

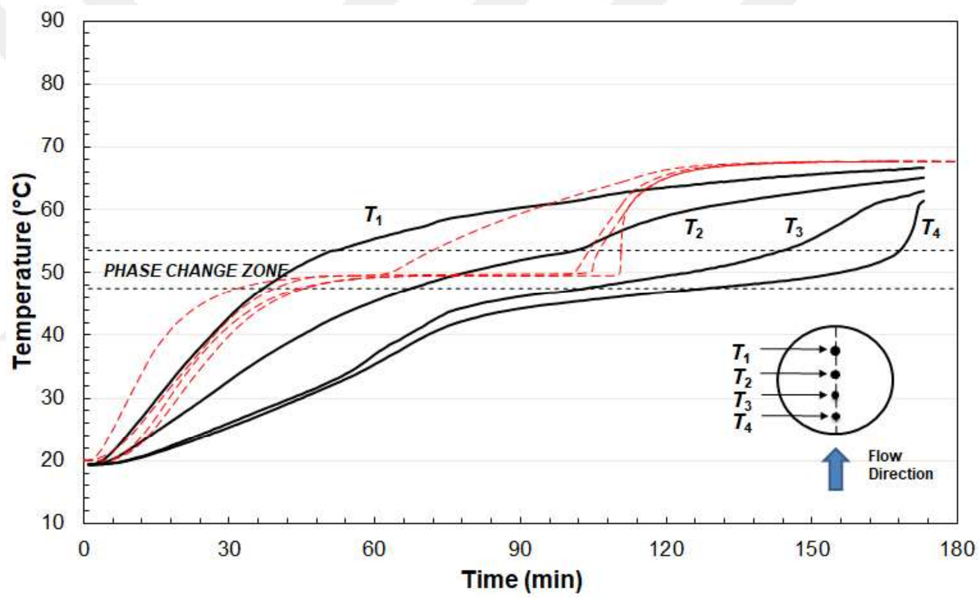

Figure 3.7 Temperature change inside capsule for T_{set} = 68°C

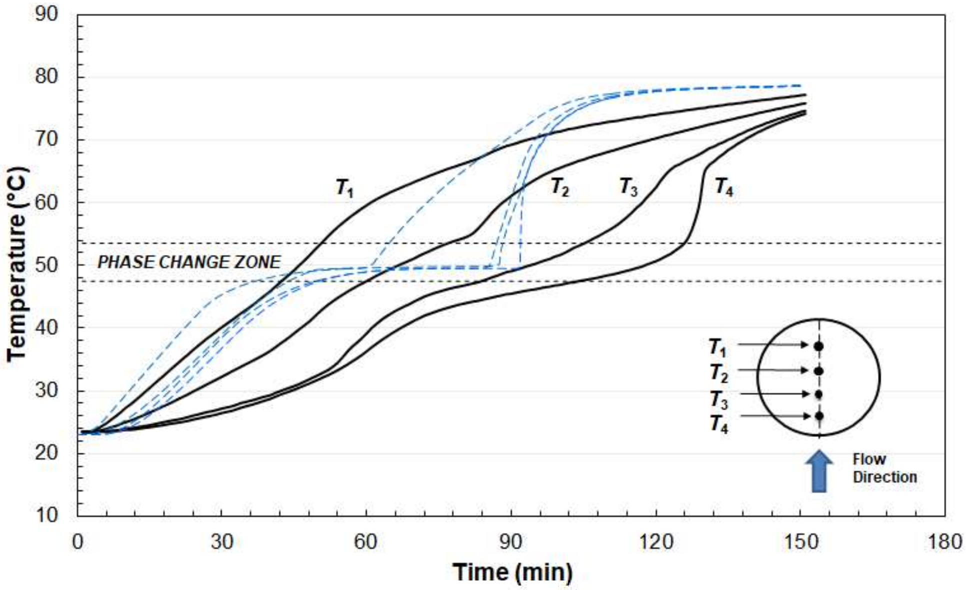

Figure 3.8 Temperature change inside capsule for T_{set} = 78°C

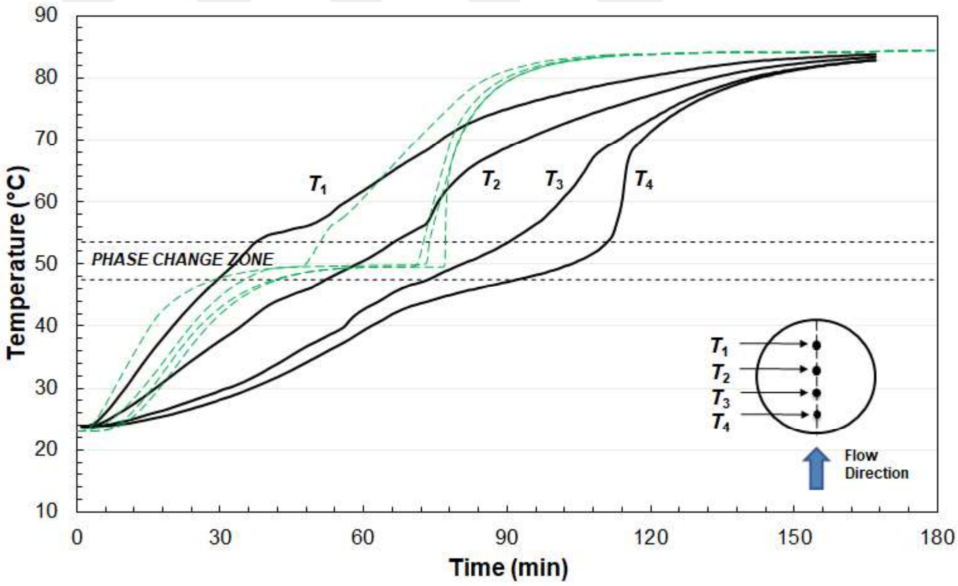

Figure 3.9 Temperature change inside capsule for T_{set} = 83°C

3.2 Inward Melting of PCM Inside In-line Spherical Capsules

3.2.1 Definition of Problem

In the current work, inward melting problem inside a cylindrical thermal energy storage tank that involves in-line arranged spherical capsules is numerically investigated. A 2D axisymmetric mathematical model is developed as illustrated in Figure 3.10. The PCM filled spheres are exposed to the cross flow with inlet velocity and temperature of U_{inlet} and T_{inlet}, respectively. All the dimensions are defined regarding the inner diameter of the spheres. The spheres have an inner diameter and a wall thickness of D_s = 80 mm and Δr = 2 mm, respectively. The model consists of six in-line arranged spheres. The distance between spheres is $2D_s$. The inner diameter of the cylindrical tube is also $2D_s$. The inlet and outlet sections of the computational domain are intentionally extended to minimize the influence of adverse pressure gradients at the inlet and outlet boundaries. A total of 27 numerical analyses are conducted by varying the inlet velocity and temperature of the working fluid, i.e., air, and the sphere shell material. The inlet temperature of the air is defined regarding the melting temperature of the PCM as T_{inlet} = T_m + 10, T_m + 15 and T_m + 20. Three different velocities of U_{inlet} = 0.5 m/s, 1.0 m/s and 3.0 m/s are studied to reveal the influence of flow field on the melting inside in-line arranged capsules. Besides, PVC, aluminum, and glass are used as the shell material. The thermophysical properties of the shell materials and the PCM are provided in Table 3.3.

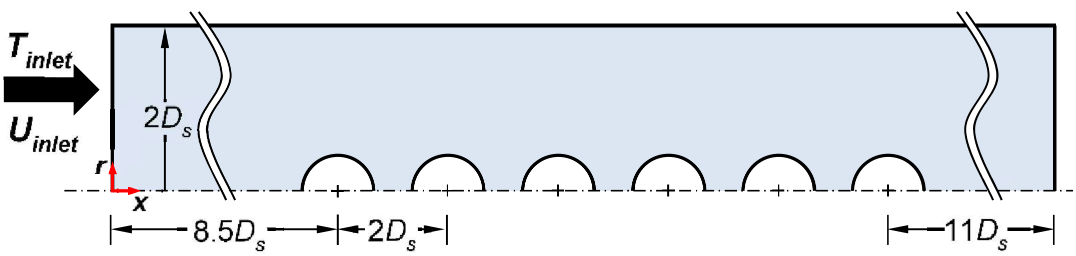

Figure 3.10 Computational domain of in-line arranged spheres with PCM

Table 3.3 Properties of spheres materials and PCM

Property	Pyrex Glass	Aluminum	PVC	PCM
Thermal conductivity, W/mK	1.4	237	0.1	0.385 (solid) 0.1505 (liquid)
Specific heat, J/kgK	835	903	840	2330
Density, kg/m^3	2225	2702	1470	772
Kinematic viscosity, m^2/s	-	-	-	5E-6
Latent heat of fusion, kJ/kg	-	-	-	243.5
Thermal expansion coefficient, K^{-1}	-	-	-	0.00091
Reference	Cengel & Ghajar (2015)			Tan et al. (2009)

3.2.2 Solution Method

The solution method of the analyses is the same as in forced convection around a single capsule. Variable parameters are given. Initially, it is assumed that temperature distribution is uniform within the computational domain as $T(r, x, t=0) = T_{init} = 26°C$. The computational domain is divided into 58534 structured computational volumes, and the grid density is increased adjacent to the no-slip surfaces. The residuals of governing equations are reduced below 10^{-8} at the end of each time-step to satisfy the convergence. Analyses are terminated when the dimensionless volume average temperature of the PCM ensures the following condition,

$$\frac{\bar{T}_{PCM} - T_{init}}{T_{inlet} - T_{init}} \geq 0.99 \tag{3.10}$$

3.2.3 Selection of the Time-Step Size

One of the crucial parameters of transient numerical analyses, when it involves the phase change phenomena, is the time-step size. Preliminary analyses are performed to determine a reasonable time-step size that provides accurate predictions that are independent of the variation in the time-step size. Figure 3.11 compares the time-wise variations of volume-averaged temperatures and liquid fractions of the PCM within the capsules #1, #2, and #6 that are evaluated under four different time-step sizes of Δt = 0.5 s, 1.0 s, 5.0 s, and 10 s. The results are overlapping, and no significant difference is observed by varying the time-step size. As an instance, at t = 100 min, regarding the liquid fraction of PCM, the differences between 0.5 s and 10 s are 0.23%, 0.23%, and 0.17% for the capsules #1, #2, and #6, respectively. Besides, the differences become 0.1%, 0.09%, and 0.01% when the results that are evaluated with Δt = 0.5 s, and 5 s are compared. One should also note that the influence of time-step size further reduces in the advancing time. As a result, time-step size of Δt =5 s is selected in the parametric runs to ensure convergence and satisfy energy balance for each of the selected working and design parameters.

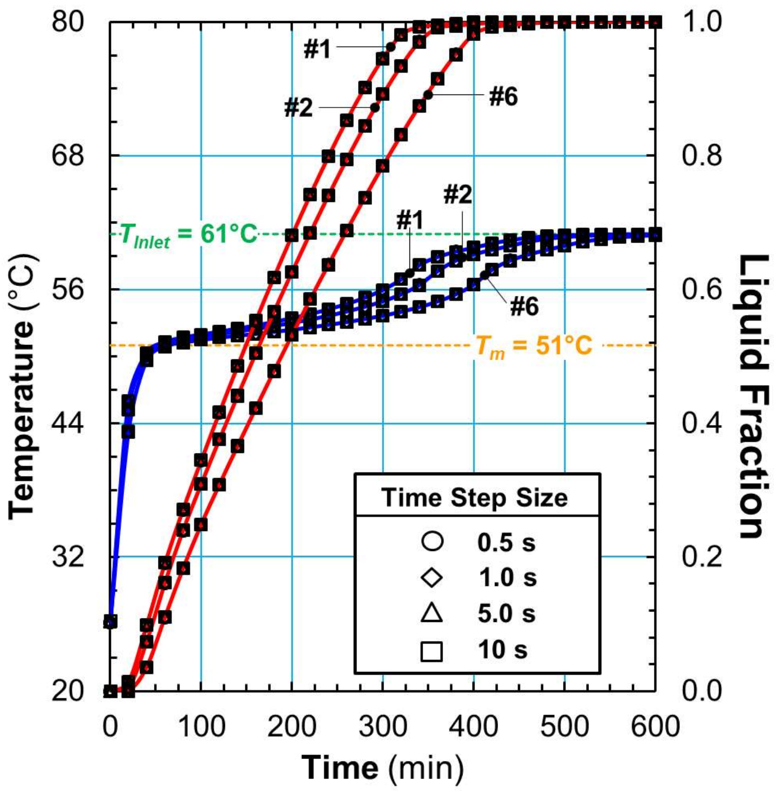

Figure 3.11 Influence of time-step size on the variations in volume-averaged PCM temperature and liquid fractions (U_{inlet} = 3 m/s and T_{inlet} = T_m +10)

3.2.4 Data Reduction

The first law and second law aspects should be considered to adequately evaluates the performance of the TES unit under various working conditions. The rate of entropy generation, $\dot{S}_{gen}$, is a measure to determine the degree of irreversibility of a system. The rate of entropy generation is evaluated by applying the following entropy balance equation,

$$\left(\dot{S}_{in}-\dot{S}_{out}\right)_{HTF}+\dot{S}_{gen}=\frac{dS}{dt} \tag{3.11}$$

where the entropy transfer by flow, *i.e.,* $\left(\dot{S}_{in}-\dot{S}_{out}\right)_{HTF}$, and the variation of the entropy within the system, *i.e., dS/dt*, are evaluated as

$$\left(\dot{S}_{in}-\dot{S}_{out}\right)_{HTF}=\left(\dot{m}c\right)_{HTF}\ln\left(\frac{T_{HTF,in}}{T_{HTF,out}}\right) \tag{3.12}$$

$$\left(\frac{dS}{dt}\right)=\left(\frac{dS}{dt}\right)_{PCM}+\left(\frac{dS}{dt}\right)_{Sphere\ Wall}+\left(\frac{dS}{dt}\right)_{HTF} \tag{3.13}$$

For the sphere wall and the HTF domains, in which the internal energy varies only in the sensible form, the variations in entropy are defined regarding the mean temperatures of the domains as $\left(\frac{dS}{dt}\right)=\left[mc\ln\left(\frac{T}{T^0}\right)\right]\Big/\Delta t$. Here Δt is the time-step size, and T^0 is the mean temperature of the domain in the previous time-step. For the PCM domain, in addition to the temperature variations, the amount of PCM that undergoes the phase transition is also included to evaluate the entropy variation as

$$\left(\frac{dS}{dt}\right)_{PCM}=\frac{\left[mc\ln\left(\frac{T}{T^0}\right)\right]_{solid}+\frac{h_{sf}}{T_m}\left(m-m^0\right)_{liquid}+\left[mc\ln\left(\frac{T}{T^0}\right)\right]_{liquid}}{\Delta t} \tag{3.14}$$

where T_m and h_{sf} indicate the melting temperature and the latent heat of fusion of the PCM.

3.2.5 Numerical Results

A total of 27 numerical analyses are conducted by varying the velocity and inlet temperature of the HTF, *i.e.,* air, and the shell material of the sphere. Results are represented regarding the fluid flow and heat transfer characteristics and the second law aspects, *i.e.,* entropy generation.

The time-averaged streamline patterns for six tandem spheres are illustrated in Figure 3.12 for three different Reynolds numbers. For Re = 1.1×10^3, 2.2×10^3 and 6.6×10^3, the corresponding inlet velocities are 0.5 m/s, 1.0 m/s and 3.0 m/s. The streamlines are generated with second-order Runge-Kutta integration of the velocity fields. The streamlines are seeded at the same location for each Reynolds number. The time-averaged flow fields produce counter-clockwise vortex street on the downstream of each sphere. It is observed that, for each Reynolds numbers, the downstream circulation bubbles resemble each other for the second, third and fourth spheres. The downstream separation region of the sphere #6 slightly extends as the flow Reynolds number increases.

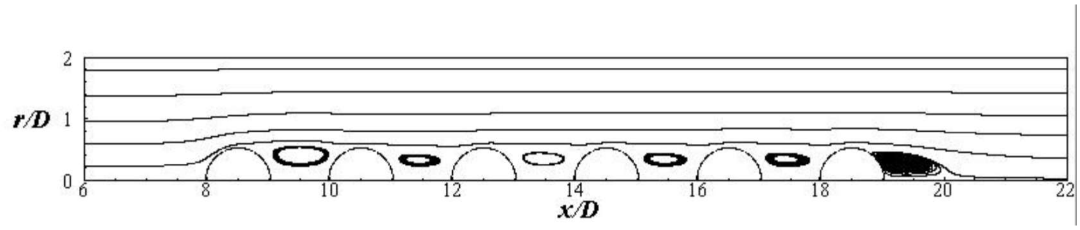

(a) Re = $1.1{\times}10^3$

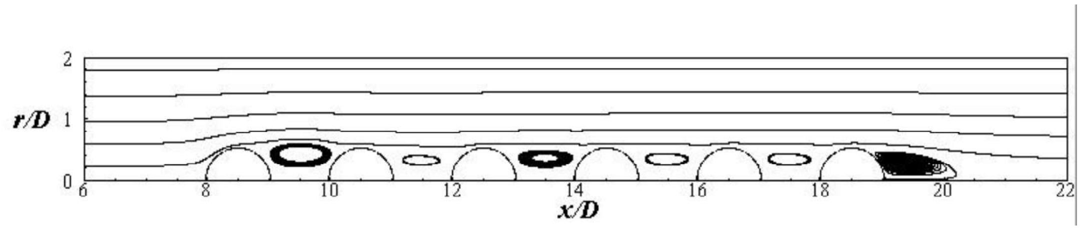

(b) Re = $2.2{\times}10^3$

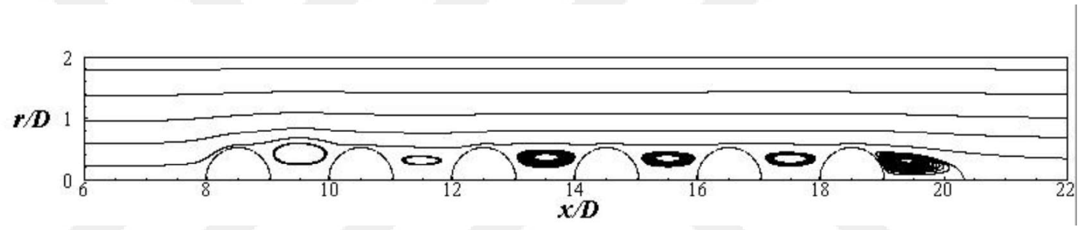

(c) Re = $6.6{\times}10^3$

Figure 3.12 Time-averaged streamlines

Figure 3.13 provides a further understanding of the flow-field. The non-dimensional axial velocity variations ($u(y)/U_{inlet}$) for three different Reynolds numbers at six dimensionless positions along the flow direction are represented. The selected positions correspond to an upstream distance of x/D = 1 from the center of each sphere. At this Reynolds regime, it is expected to observe a laminar boundary layer separation, and the separated shear layer produces a small-scale turbulent wake flow (Kravchenko & Moin, 2000). However, as introduced by Zhou & Yiu (2006), the time-averaged mean velocity profiles correspond to a single turbulent vortex shedding on the downstream of each sphere (see Figure 3.13). The velocity profiles are not significantly influenced by the variation of Reynolds number from $1.1{\times}10^3$ to $6.6{\times}10^3$. The most significant difference between the velocity profiles is observed behind the first sphere especially in the range of $0 \le r/D \le 0.5$ (see Figure 3.13 (b)).

In this range, the minimum value of the dimensionless velocity increases from -0.5 to -0.8 as the flow Reynolds number increases. Notice that for the upstream position of the second sphere the zero velocity, or the center of the recirculation zone, is observed approximately at r/D = 0.5. For the rest of the spheres, from spheres #3 to #6, the velocity profiles at the upstream locations are almost overlapping, and the center of the recirculation zones slightly shift below r/D = 0.5. On the axis plane, r/D = 0, the dimensionless velocities are about -0.3 and reach the free stream velocity around r/D = 0.8.

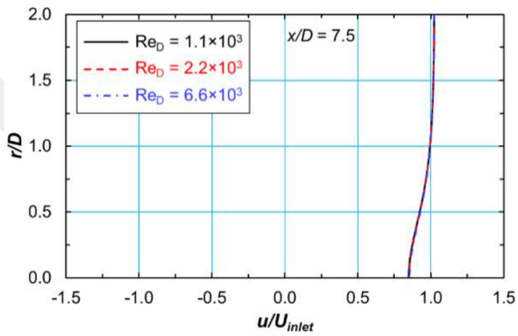

(a) Sphere #1

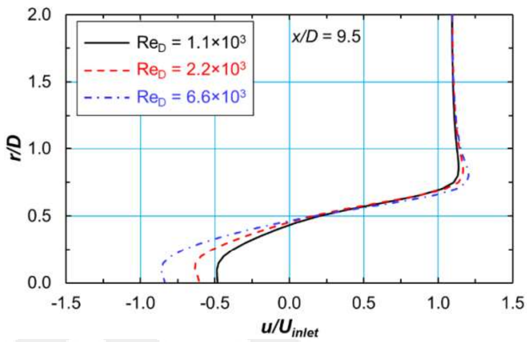

(b) Sphere #2

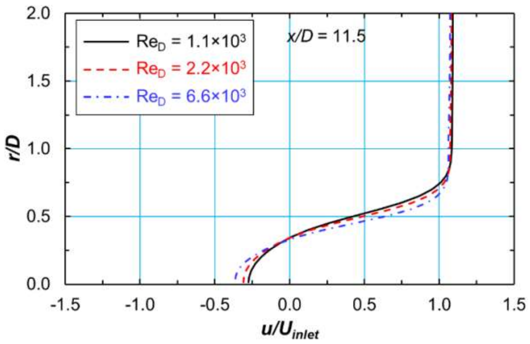

(c) Sphere #3

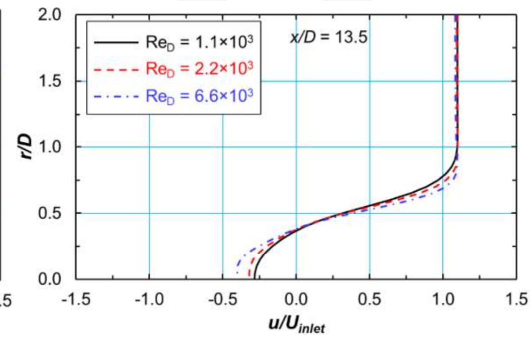

(d) Sphere #4

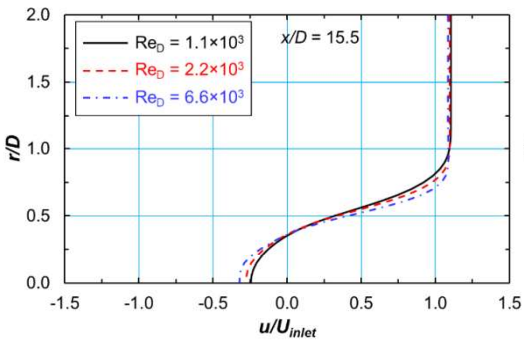

(e) Sphere #5

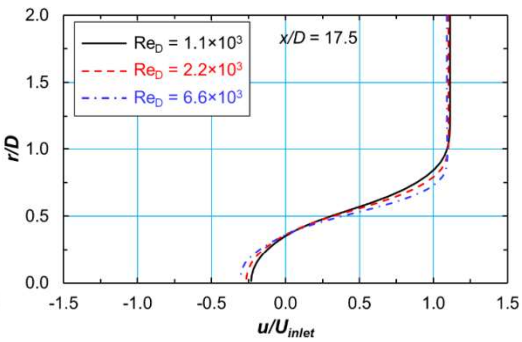

(f) Sphere #6

Figure 3.13 Mean axial velocity profiles at upstream positions of spheres

Figures 3.14 (a) to (c) reveal the influence of inlet temperature on the variations of mean temperature and the liquid fractions PCMs inside the selected spheres. In Figure 3.14 (d), on the other hand, the time-wise variations of the entropy generations are given at three inlet temperatures. In this set of analyses, the shell material is glass, and the flow Reynolds number is 1.1×10^3. From Figures 3.14 (a) to (c), one can infer that the charging process consists of three sub-processes as *(i)* solid PCM's sensible heating, *(ii)* melting and *(iii)* liquid PCM's sensible heating. Notice that the mean temperature of PCM quickly increases in the early period of the charging period and reaches the melting temperature before t = 50 min. During this period, the internal energy variation of the PCM is mainly sensible heating. It is interesting to note that the inlet temperature of the HTF has no significant influence on the variations of the PCM temperature during the sensible heating period. However, as the amount of liquid PCM within the spheres increases, the influence of inlet temperature of the HTF on the temperature variations becomes remarkable. The melting process accelerates as the inlet temperature increases, as it is expected. The slopes of the temperature curves become steeper, and the complete melting is achieved more quickly, as long as the various between the inlet temperature of the HTF and the melting temperature of the PCM increases. As an instance, for the sphere #1, the complete melting observed at approximately t = 300 min, 400 min, and 550 min, for the inlet temperatures of $T_m + 20$, $T_m + 15$ and $T_m + 10$, respectively. Notice that based on the sensible heating period of the PCM and the shell material, the PCM temperatures require further time beyond the complete melting to approach the inlet temperature of the HTF. The rate of heat transfer inside the spheres significantly reduces along the flow direction. For instance, regarding the time for complete melting, the difference between sphere #1 and #6 is almost 150 min at T_m + 20. Figure 3.14 (d) indicates the influence of the inlet temperature of the HTF on the rate of entropy generation. Entropy generation's rate significantly increases as the inlet temperature increases since the spatial temperature gradients, or irreversibilities due to the finite temperature difference, within the spheres also increase. Notice that in the early periods of the charging process, *i.e.,* sensible heating period, the rate of entropy generation reduces dramatically. On the other hand, during the phase change period, the entropy generation rate remains almost constant with slight fluctuations.

As the phase change process is completed, the rate of entropy generation approaches through zero. Even though increasing the variation between the inlet temperature of the HTF and the melting temperature of the PCM significantly improves the heat transfer process, one should keep in mind that the entropy generation rate, or the irreversibilities, increases remarkably.

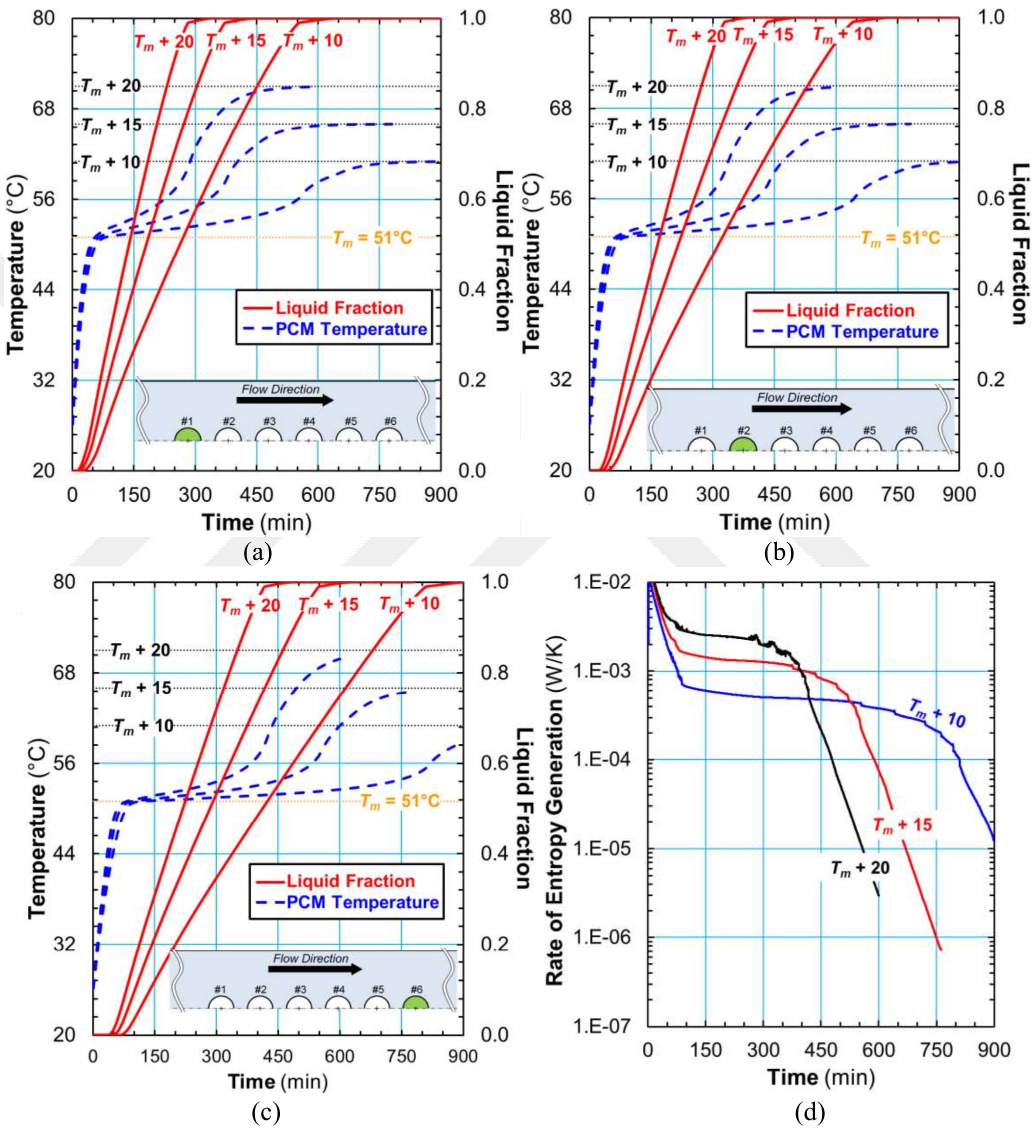

Figure 3.14 Effect of the inlet temperature on the heat transfer inside (a) Sphere #1, (b) Sphere #2, and (c) Sphere #6 and (d) the rate of entropy generation – Re = 1.1×10^3

In Figure 3.15 the liquid fraction contours are given at three selected instances, *i.e.,* t = 75 min, 150 min, and 225 min, for spheres #1, #2 and #6. The results are given for moderate inlet temperature, $T_{inlet} = T_m + 10$. The liquid fraction gradually increases in each sphere in advancing time. It is clear that the flow field significantly influences the evolution of the melting process and the interface front varies along the angular position, θ. For the sphere #1, at the early stage of the charging process, *i.e.,* t = 75 min, the melting initiates at the upstream ($\theta = 0°$) and downstream ($\theta = 180°$) stagnation points. The penetration of the liquid PCM is deeper at $\theta = 0°$, and the rate of melting reduces along $\theta = 90°$. Notice that the rate of melting significantly reduces beyond 90° due to the separation of the flow and the reduced local Nusselt number on the sphere surface. The weak recirculation region at the rear side of the sphere slightly improves the local Nusselt number near 180°. A nonuniform interface front is observed at the end of 225 min. The separation of flow across the sphere wall slows down the melting process between $120° < \theta < 145°$. For the sphere #2, on the other hand, the melting process initiates at the upper region, $30° < \theta < 100°$, of the sphere. The circulation cells that are observed at the upstream and downstream of the sphere #2 significantly reduces the melting of PCM for the angular positions of $0° < \theta < 45°$ and $120° < \theta < 145°$. It is interesting to note that for the sphere #2, the interface position at $\theta = 90$ is almost identical with $\theta = 180°$. The interface variation in sphere #6 has a similar behavior as in sphere #2, but the rate of melting is lower in sphere #6. Spatial and temporal solid/liquid interface variations clearly show that the melting process inside the spheres significantly governed by the flow field around the spheres.

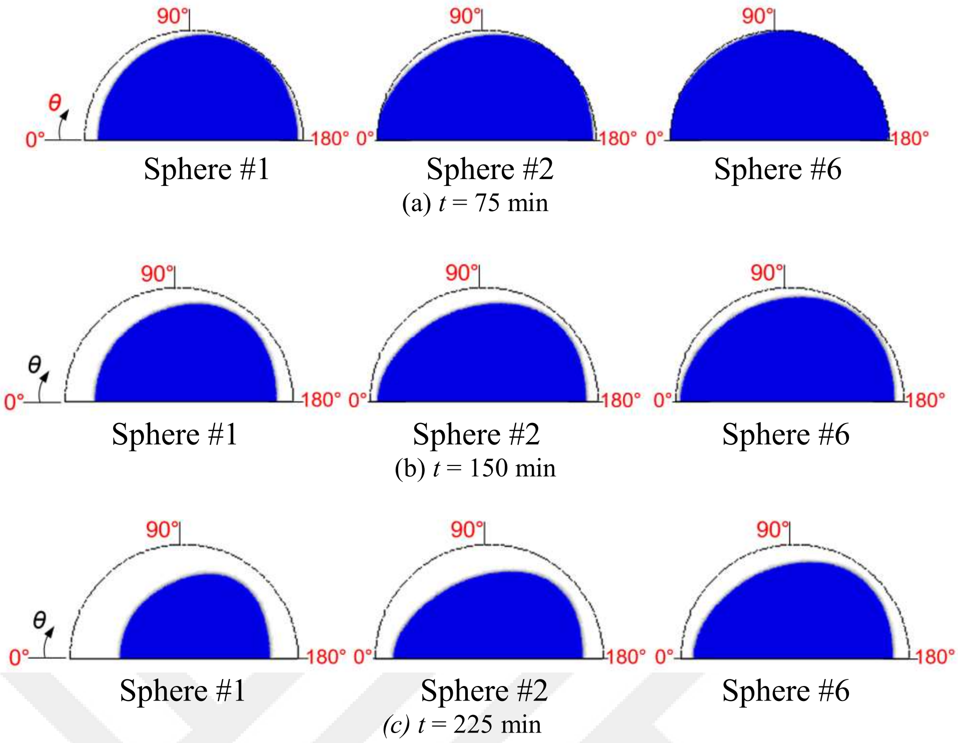

Figure 3.15 Evolution of the liquid fraction of spheres #1, #2, #6 for $T_{inlet} = T_m + 10$ (*white*: liquid PCM, *blue*: solid PCM)

In Figures 3.16 (a) to (c), the influence of capsule material on the heat transfer process of the PCM is represented for spheres #1, #2, and #6. Regardless of the shell material of the capsules, the variations in the PCM temperature and a liquid fraction are almost identical at the early periods of the charging process, *i.e.,* t < 100 min. When the temperature of the sphere exceeds the melting temperature of the PCM the influence of the shell material becomes apparent. The capsule material with high thermal conductivity improves the rate of heat transfer enhances as, as it is expected. The liquid fraction reaches to the unity slightly faster for the case in which aluminum is used as the shell material. However, one should notice that even though the thermal conductivity of aluminum is more than one hundred times higher than the glass (see Table 3.3), there is no remarkable difference between the glass and aluminum shell materials regarding the time-wise variations of the liquid fraction and mean temperature of the PCM. This fact is due to the order of thermal resistivities inside and outside the spherical capsules. The conductive resistance of the glass sphere wall has the same order of magnitude of the convective resistance of the forced convection around the spherical capsules. The conductive resistance further reduces when aluminum is used as the shell material, but it has a slight impact on the time-wise variations of the liquid fraction, or temperature since the heat transfer is mainly governed by the convective resistance around the spheres when the conductive resistance within the shell material dropped below a certain value. In the case of the PVC, on the other hand, the conductive resistance of the shell material becomes higher than the convective resistance around the spheres, that is the heat transfer process significantly reduces. One should notice that rather than the thermal diffusivity, the thermal conductivity of the shell material plays a significant role on the transient heat transfer since the thermal mass of the sphere wall relatively small when it is compared with the sensible and latent heat capacities of the PCM. Figure 3.16 (d) shows that the rate of entropy generation scales up as the thermal conductivity of the shell material increases. Even though the variations in entropy generation rate look closer during the sensible heating of the solid PCM and the phase change process, *i.e.,* $t < 450$ min, a close look to the dataset clearly shows that the rate of entropy generation is more than seven times higher for the aluminum spheres when it is compared with the ones with glass or PVC. One may expect this finding since the temperature gradients inside the PCM domain increase as the sphere wall temperature reaches to the HTF free stream temperature more quickly.

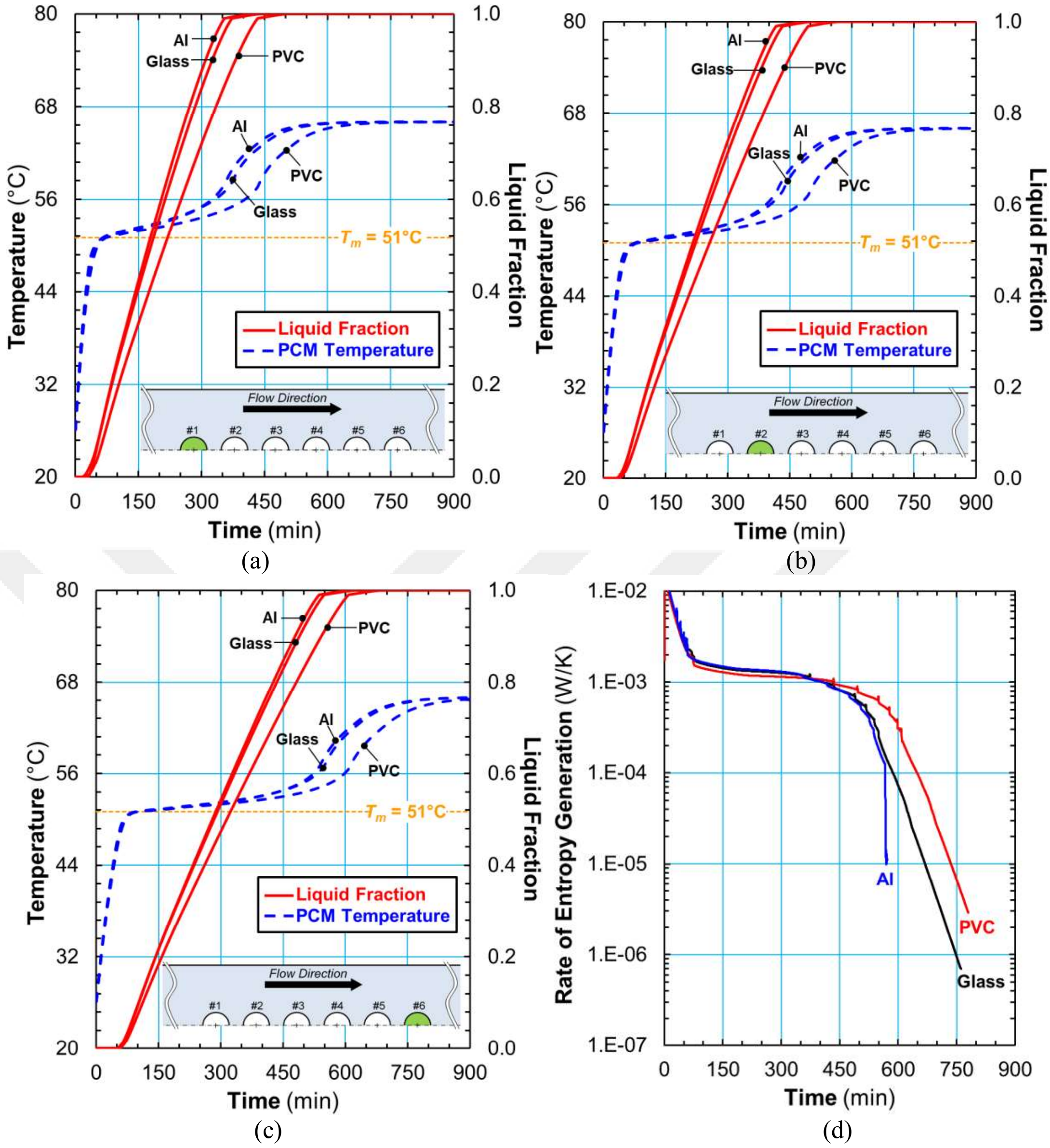

Figure 3.16 Effect of the sphere shell material on the heat transfer inside (a) Sphere #1, (b) Sphere #2, and (c) Sphere #6 and (d) the rate of entropy generation – Re = 1.1×10^3

Figures 3.17 (a) to (c) show the influence of inlet velocity of the HTF on the time-wise variations of the PCM temperature and liquid fraction. The speed of charging process increases as the inlet velocity increases, as it is expected. Increasing the inlet velocity of the HTF improves the convective heat transfer coefficient around spherical capsules. That is the rate of melting enhances. For the sphere #1, the time for complete melting is attained as 250 min, 325 min and 400 min, for HTF velocities of 3.0 m/s, 1.0 m/s and 0.5 m/s, respectively. Notice that the influence of inlet velocity becomes remarkable for the spheres that are located at the downstream. For sphere #6, as an instance, the time for complete melting becomes 300 min, 450 min, and 600 min, for HTF velocities of 3.0 m/s, 1.0 m/s and 0.5 m/s, respectively. Increasing the velocity of the HTF also increases the irreversibilities of the system. Figure 3.17 (d) depicts that the rate of entropy generation increases more than twice when the velocity is increased from 0.5 m/s to 3.0 m/s.

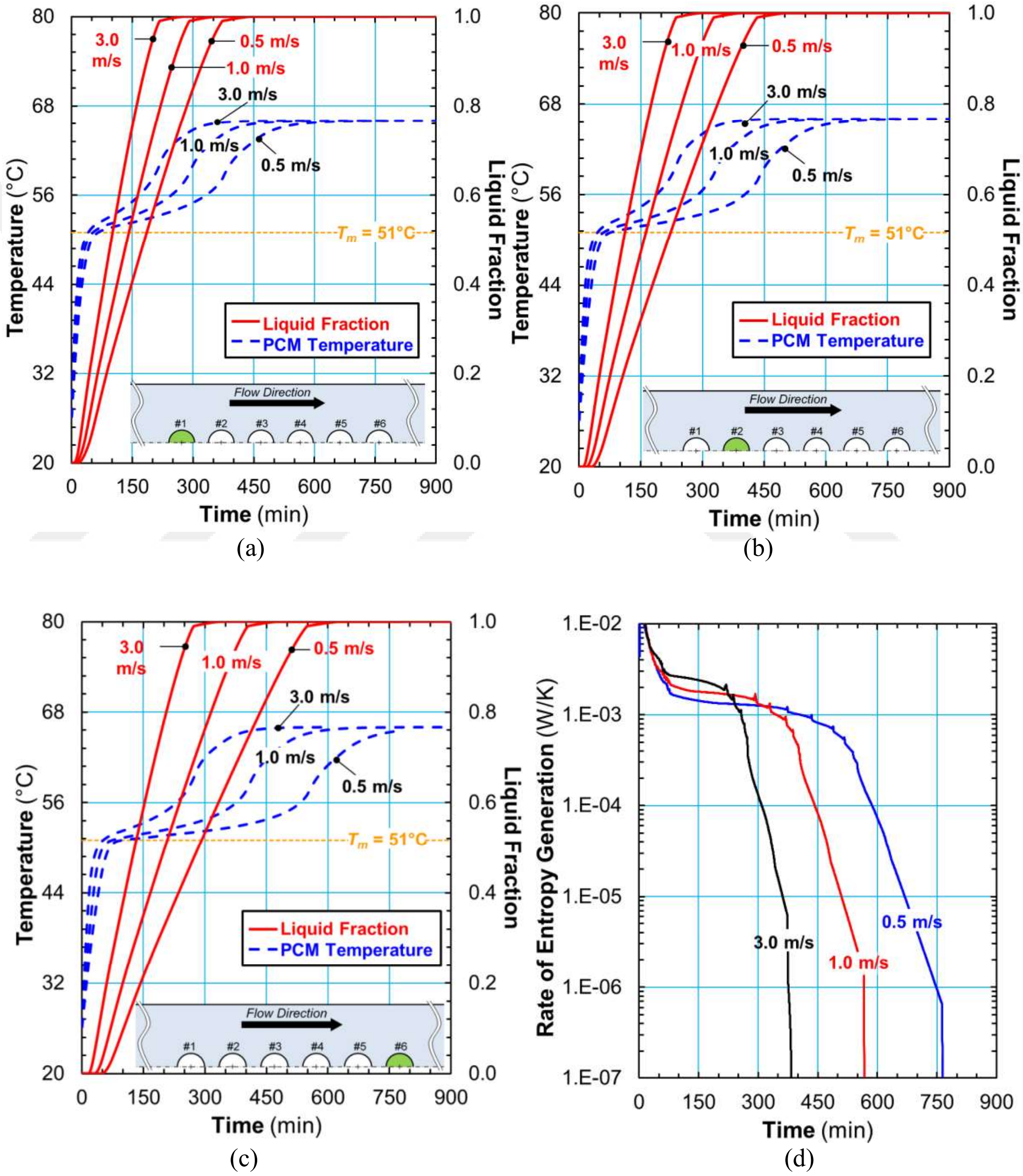

Figure 3.17 Effect of the HTF velocity on the heat transfer inside (a) Sphere #1, (b) Sphere #2, and (c) Sphere #6 and (d) the rate of entropy generation – Re = 1.1×10^3

In Table 3.4 the average values of the rate of heat transfer and rate of entropy generation are given for each design and working condition of the LHTES unit which consist of in-line spherical capsules. The process time is determined according to the definition given in Equation (3.10). Notice that increasing the inlet temperature, or the velocity, of the HTF, improves the rate of heat transfer and reduces the duration for charging. However, such an increment in heat transfer speed also increases the entropy generation, or the irreversibilities, of the storage unit. Current results clearly show that dealing only with the first law aspects is not enough to determine the real performance of an LHTES system. Operating the system at higher temperatures or circulating the HTF at high velocities, for sure, lead the loss of quality of energy. The irreversibilities, or the quality loss of energy, can only be utilized by considering the second law aspects of the thermodynamics. Optimum design and working parameters, therefore, should be evaluated to minimize the entropy generation and maximize the rate of heat transfer.

Table 3.4 Effect of the working and design parameters on the average rate of heat transfer and rate of entropy generation

Case #	**Shell material**	T_{inlet}	U_{inlet} (m/s)	$t_{process}$ (min)	**Average Heat Transfer Rate** (W)	**Average Entropy Generation Rate** (W/K)
1	Glass	$T_m + 10$	0.5	900	7.9	1.12E-02
2			1.0	777	9.2	1.30E-02
3			3.0	550	13.0	1.83E-02
4		$T_m + 15$	0.5	780	9.6	1.34E-02
5			1.0	590	12.7	1.77E-02
6			3.0	415	18.0	2.51E-02
7		$T_m + 20$	0.5	600	12.9	1.80E-02
8			1.0	499	15.5	2.17E-02
9			3.0	351	22.0	3.09E-02
10	PVC	$T_m + 10$	0.5	1066	6.6	9.45E-03
11			1.0	887	8.0	1.14E-02
12			3.0	660	10.7	1.52E-02
13		$T_m + 15$	0.5	864	8.5	1.20E-02
14			1.0	673	11.0	1.54E-02
15			3.0	500	14.7	2.08E-02
16		$T_m + 20$	0.5	731	10.5	1.47E-02
17			1.0	569	13.4	1.89E-02
18			3.0	423	18.1	2.54E-02
19	Al	$T_m + 10$	0.5	1014	7.2	9.97E-03
20			1.0	766	9.5	1.32E-02
21			3.0	545	13.3	1.85E-02
22		$T_m + 15$	0.5	772	9.8	1.35E-02
23			1.0	581	13.0	1.79E-02
24			3.0	411	18.4	2.54E-02
25		$T_m + 20$	0.5	655	12.0	1.64E-02
26			1.0	493	16.0	2.18E-02
27			3.0	348	22.6	3.09E-02

CHAPTER FOUR
CONCLUSION

In chapter two, the PCM storage (melting) process in the spherical capsule is examined experimentally. In this context, experiments were executed for three different set points of air inlet temperature. The mean values for the set temperatures of 68°C, 78°C and 83°C were obtained 61.58°C, 68.64°C and 75.18°C, respectively. The main results are as follows:

- Increasing the inlet temperature from the set value of 68°C to the set value of 83°C, the time needed to finalize the melting of the PCM is reduced by approximately 55%.
- The melting process in the spherical capsule takes place downstream of the neck. The local convection coefficient around the capsule, the free convection within the air in the neck and the natural convection movement of the melting PCM cause a vertical melting.

Chapter three focuses on investigating the melting process of PCM in spherical capsules using an enhanced thermal conductivity correlation under various working conditions. A novel approach is implemented in ANSYS-FLUENT software to incorporate the influence of natural convection without resolving the flow-field equations in the liquid PCM domain. Both first law and second law aspects are considered to detect the influences of working and design parameters of the LHTES unit. The conclusions of the study are summarised as

- The UDF code that is developed in this work accurately predicts the variation of the liquid fraction; the maximum error is less than 10%.
- Increasing the inlet temperature or the velocity of HTF increases the heat transfer rate and reduces the time for complete melting but the entropy generation rate, or irreversibility of the storage unit, significantly increases.
- The current results indicate that the first law aspects, *i.e.,* evaluating the rate of heat transfer or total time for melting, is not enough alone to determine the actual performance of an LHTES system the irreversibilities of the system

should also be taken into account as the primary objective in the optimization procedure.

Implementation of enhanced thermal conductivity approach in the mathematical models of real scale LHTES models will, for sure, reduce the computational cost and develop the accuracy of the predictions.

REFERENCES

Adine, H. A., & El Qarnia, H. (2009). Numerical analysis of the thermal behaviour of a shell-and-tube heat storage unit using phase change materials. *Applied Mathematical Modelling*, *33*(4), 2132-2144.

Amin, N. A. M., Bruno, F., & Belusko, M. (2014). Effective thermal conductivity for melting in PCM encapsulated in a sphere. *Applied Energy*, *122*, 280-287.

Archibold, A. R., Gonzalez-Aguilar, J., Rahman, M. M., Goswami, D. Y., Romero, M., & Stefanakos, E. K. (2014). The melting process of storage materials with relatively high phase change temperatures in partially filled spherical shells. *Applied Energy*, *116*, 243-252.

Assis, E., Katsman, L., Ziskind, G., & Letan, R. (2007). Numerical and experimental study of melting in a spherical shell. *International Journal of Heat and Mass Transfer*, *50*(9-10), 1790-1804.

Bechiri, M., & Mansouri, K. (2015). Analytical solution of heat transfer in a shell-and-tube latent thermal energy storage system. *Renewable Energy*, *74*, 825-838.

Bellan, S., Alam, T. E., González-Aguilar, J., Romero, M., Rahman, M. M., Goswami, D. Y., & Stefanakos, E. K. (2015). Numerical and experimental studies on heat transfer characteristics of thermal energy storage system packed with molten salt PCM capsules. *Applied Thermal Engineering*, *90*, 970-979.

Cárdenas, B., & León, N. (2013). High temperature latent heat thermal energy storage: Phase change materials, design considerations and performance enhancement techniques. *Renewable and Sustainable Energy Reviews*, *27*, 724-737.

Cengel, Y. & Ghajar, A. J. (2014). *Heat and Mass Transfer: Fundamentals and Applications* (5th ed). New York: McGraw-Hill Higher Education.

Chan, C. W., & Tan, F. L. (2006). Solidification inside a sphere—an experimental study. *International Communications in Heat and Mass Transfer*, *33*(3), 335-341.

Chiu, C. P., & Chen, W. R. (1996). Transient natural convection heat transfer between concentric and vertically eccentric spheres. *International Journal of Heat and Mass Transfer*, *39*(7), 1439-1452.

Cho, K., & Choi, S. H. (2000). Thermal characteristics of paraffin in a spherical capsule during freezing and melting processes. *International Journal of Heat and Mass Transfer*, *43*(17), 3183-3196.

Ettouney, H., El-Dessouky, H., & Al-Ali, A. (2005). Heat transfer during phase change of paraffin wax stored in spherical shells. *Transactions-American Society of Mechanical Engineers Journal of Solar Energy Engineering*, *127*(3), 357.

Ezan, M. A., Uzun, M., & Erek, A. (2014). A study on evaluation of effective thermal conductivity for spherical capsules. *International Conference on Heat Transfer, Fluid Mechanics and Thermodynamics.*

Farid, M., Kim, Y., Honda, T., & Kanzawa, A. (1989). The role of natural convection during melting and solidification of PCM in a vertical cylinder. *Chemical Engineering Communications*, *84*(1), 43-60.

Hariharan, K., Kumar, G. S. S., Kumaresan, G., & Velraj, R. (2018). Investigation on phase change behavior of paraffin phase change material in a spherical capsule for solar thermal storage units. *Heat Transfer Engineering*, *39*(9), 775-783.

Hasnain, S. M. (1998). Review on sustainable thermal energy storage technologies, Part I: heat storage materials and techniques. *Energy Conversion and Management*, *39*(11), 1127-1138.

Ismail, K. A. R., & Henrıquez, J. R. (2002). Numerical and experimental study of spherical capsules packed bed latent heat storage system. *Applied Thermal Engineering*, *22*(15), 1705-1716.

Iten, M., & Liu, S. (2014). A work procedure of utilising PCMs as thermal storage systems based on air-TES systems. *Energy Conversion and Management*, *77*, 608-627.

Jian-you, L. (2008). Numerical and experimental investigation for heat transfer in triplex concentric tube with phase change material for thermal energy storage. *Solar Energy*, *82*(11), 977-985.

Karthikeyan, S., & Velraj, R. (2012). Numerical investigation of packed bed storage unit filled with PCM encapsulated spherical containers–a comparison between various mathematical models. *International Journal of Thermal Sciences*, *60*, 153-160.

Karthikeyan, S., Solomon, G. R., Kumaresan, V., & Velraj, R. (2014). Parametric studies on packed bed storage unit filled with PCM encapsulated spherical containers for low temperature solar air heating applications. *Energy Conversion and Management*, *78*, 74-80.

Khadiran, T., Hussein, M. Z., Zainal, Z., & Rusli, R. (2016). Advanced energy storage materials for building applications and their thermal performance characterization: A review. *Renewable and Sustainable Energy Reviews*, *57*, 916-928.

Khot, S. A., Sane, N. K., & Gawali, B. S. (2011). Experimental investigation of phase change phenomena of paraffin wax inside a capsule. *International Journal of Engineering Trends and Technology*, *2*(2).

Kravchenko, A. G., & Moin, P. (2000). Numerical studies of flow over a circular cylinder at Re D= 3900. *Physics of Fluids*, *12*(2), 403-417.

Li, W., Wang, Y. H., & Kong, C. C. (2015). Experimental study on melting/solidification and thermal conductivity enhancement of phase change material inside a sphere. *International Communications in Heat and Mass Transfer*, *68*, 276-282.

Liao, Z., Xu, C., Ren, Y., Gao, F., Ju, X., & Du, X. (2018). A novel effective thermal conductivity correlation of the PCM melting in spherical PCM encapsulation for the packed bed TES system. *Applied Thermal Engineering*, *135*, 116-122.

Liu, M. J., Fan, L. W., Zhu, Z. Q., Feng, B., Zhang, H. C., & Zeng, Y. (2016). A volume-shrinkage-based method for quantifying the inward solidification heat transfer of a phase change material filled in spherical capsules. *Applied Thermal Engineering*, *108*, 1200-1205.

Patankar, S. (1980). *Numerical Heat Transfer and Fluid Flow*. New York: McGraw-Hill.

Rathod, M. K., & Banerjee, J. (2013). Thermal stability of phase change materials used in latent heat energy storage systems: a review. *Renewable and Sustainable Energy Reviews*, *18*, 246-258.

Raul, A., Jain, M., Gaikwad, S., & Saha, S. K. (2018). Modelling and experimental study of latent heat thermal energy storage with encapsulated PCMs for solar thermal applications. *Applied Thermal Engineering*, *143*, 415-428.

Regin, A. F., Solanki, S. C., & Saini, J. S. (2008). Heat transfer characteristics of thermal energy storage system using PCM capsules: a review. *Renewable and Sustainable Energy Reviews*, *12*(9), 2438-2458.

Regin, A., Solanki, S. C., & Saini, J. S. (2006). Experimental and numerical analysis of melting of PCM inside a spherical capsule. *9th AIAA/ASME Joint Thermophysics and Heat Transfer Conference*, 3618.

Sarı, A., & Karaipekli, A. (2007). Thermal conductivity and latent heat thermal energy storage characteristics of paraffin/expanded graphite composite as phase change material. *Applied Thermal Engineering*, *27*(8-9), 1271-1277.

Scanlan, J. A., Bishop, E. H., & Powe, R. E. (1970). Natural convection heat transfer between concentric spheres. *International Journal of Heat and Mass Transfer*, *13*(12), 1857-1872.

Tan, F. L. (2008). Constrained and unconstrained melting inside a sphere. *International Communications in Heat and Mass Transfer*, *35*(4), 466-475.

Tan, F. L., Hosseinizadeh, S. F., Khodadadi, J. M., & Fan, L. (2009). Experimental and computational study of constrained melting of phase change materials (PCM) inside a spherical capsule. *International Journal of Heat and Mass Transfer*, *52*(15-16), 3464-3472.

Tao, Y. B., & He, Y. L. (2011). Numerical study on thermal energy storage performance of phase change material under non-steady-state inlet boundary. *Applied Energy*, *88*(11), 4172-4179.

Tao, Y. B., He, Y. L., & Qu, Z. G. (2012). Numerical study on performance of molten salt phase change thermal energy storage system with enhanced tubes. *Solar Energy*, *86*(5), 1155-1163.

Tao, Y. B., He, Y. L., Cui, F. Q., & Lin, C. H. (2013). Numerical study on coupling phase change heat transfer performance of solar dish collector. *Solar Energy*, *90*, 84-93.

Theory Reference ANSYS release 16.2.3 (n.d.). Retrieved April 9, 2019, from https://www.sharcnet.ca/Software/Ansys/16.2.3

Voile, V., & Prakash, C. (1987). A fixed grid numerical modeling methodology for convection diffusion mushy region phase-change problem. *International Journal Heat Mass Transfer*, *30*(9), 1709-1719.

Wu, S., & Fang, G. (2011). Dynamic performances of solar heat storage system with packed bed using myristic acid as phase change material. *Energy and Buildings*, *43*(5), 1091-1096.

Zhou, Y., & Yiu, M. W. (2006). Flow structure, momentum and heat transport in a two-tandem-cylinder wake. *Journal of Fluid Mechanics*, *548*, 17-48.

APPENDICES

NOMENCLATURE

A	surface area (m^2)
c	specific heat (J/kgK)
D_s	inner diameter (m)
g	gravity (m/s^2)
H	total enthalpy (J/kg)
h	specific enthalpy (J/kg)
h_{sf}	latent heat of fusion (kJ/kg)
k	thermal conductivity (W/mK)
$\dot{m}$	mass flow rate (kg/s)
Nu	Nusselt number (-)
P	pressure (Pa)
Pr	Prandtl number (-)
R	universal gas constant (kJ/kgK)
Ra	Rayleigh number (-)
Re	Reynolds number (-)
r	radial coordinate (m)
r_{eq}	equivalent interface radius (m)
$\dot{S}_{gen}$	rate of entropy generation (W/K)
T	temperature (K or °C)
$\overline{T}_{wall}$	mean temperature (K or °C)
t	time (s)
U	velocity (m/s)
V	velocity (m/s)
x	axial coordinate (m)
Q	volume rate (m^3/s)

Greek letters

β	thermal expansion coefficient (K^{-1})
Δt	time-step size (s)
Δr	shell thickness (m)
δ	gap spacing (m)
μ	dynamic viscosity (kg/ms)
ϑ	kinematic viscosity (m^2/s)
ρ	density (kg/m^3)

Subscripts

init	initial
l	liquid phase
m	melting
ref	reference
s	solid phase
t	turbulent

wall	inner sphere surface

Superscripts

^{0}	previous time

Abbreviations

HTF	heat transfer fluid
LHTES	latent heat thermal energy storage
PCM	phase change material
TES	thermal energy storage
UDF	user-defined-function
DSC	differential scanning calorimetry